Cell surface localisation of GPI-anchored receptors in *Trypanosoma brucei*

Sourav Banerjee[1*], Nicola Minshall[1*], Alexander D Cook[2,3], Olivia Macleod[1], Helena Webb[1], Matthew Higgins[2,3] and Mark Carrington[1]

[1] Department of Biochemistry, University of Cambridge, Tennis Court Road, Cambridge CB2 1QW, UK.

[2] Department of Biochemistry, University of Oxford, South Parks Road, Oxford OX1 3QU, UK.

[3]Kavli Institute for Nanoscience Discovery, Dorothy Crowfoot Hodgkin Building, University of Oxford, South Parks Rd, Oxford, OX1 3QU, UK.

* These authors made equal contributions

Correspondence: Mark Carrington: mc115@cam.ac.uk

ABSTRACT

Trypanosoma brucei, the causal agent of Human and Animal African trypanosomiasis proliferates in the extracellular milieu of mammals. It acquires host macromolecular nutrients, by receptor mediated endocytosis. The best characterised cell surface receptor is for transferrin (TfR) and it has been reported to be preferentially localised in the flagellar pocket domain of the plasma membrane, the sole site of endocytosis. In this location the TfR may be inaccessible to adaptive immune system effectors. The *T. brucei* genome encodes ~15 TfR variants, and here we compared two, the first attached to the plasma membrane by a single glycosylphosphatidylinositol (GPI)-anchor and the other by two. Transferrin uptake kinetics were similar and rapid for both. Unexpectedly, initial binding of transferrin occurred over the whole cell surface suggesting the TfR was not localised solely in the flagellar pocket. This localisation was confirmed by immunofluorescence assays and was independent of the number of GPI-anchors. Two other GPI-anchored receptors were investigated to determine whether localisation to the whole cell surface was a general property of GPI-anchored receptors. Haptoglobin-haemoglobin uptake assays and immunofluorescence localisation of complement factor H receptor showed both were also whole cell surface localised. The mechanisms by which trypanosome receptors are protected from antibody-mediated attack are more complex than hiding in a pocket.

INTRODUCTION

Trypanosoma brucei proliferates within the bloodstream and tissue spaces of mammals and can maintain a long-term infection lasting in some cases for years. To do this, it must avoid the host adaptive and innate immune response at the same time as acquiring nutrients from the host. The adaptive immune response is overcome through a population survival strategy based on a densely packed surface coat of variant surface glycoprotein (VSG) that undergoes antigenic variation. As the antibody titre against one VSG increases, a small subset of trypanosomes that have switched expression to a different VSG escape until they are recognised in turn and so on in an iterative process (Mugnier et al., 2015). The trypanosome has evolved mechanisms to increase the titre of host immunoglobin required for killing. First, there is rapid endocytosis and degradation of VSG bound antibody (Engstler et al., 2007) and second, a receptor for IgG Fc region (ISG75) (Mikkelsen et al., 2024). How the innate immune system is countered is less well understood (Pinger et al., 2018) but receptors for Complement C3, known as ISG65, and Factor H (FHR) have been identified and characterised (Cook et al., 2024; Macleod et al., 2020, 2022). Acquisition of small molecule nutrients, such as glucose and amino acids, use typical eukaryotic membrane transporters.

Obtaining host macromolecule nutrients poses a more complex problem. First, *T. brucei* has a very wide host range and presumably receptors recognise ligands from a range of host species, this has been shown to be the case for the transferrin (TfR) (Trevor et al., 2019). Second, as the TfR and haptoglobin haemoglobin receptor (HpHbR) (Lane-Serff et al., 2016) bind ligands that have similar dimensions to immunoglobulin molecules then why are host antibodies against receptors not sufficient to clear an infection? Some models to account for this suggested that the VSG coat acts as a barrier preventing immunoglobulin access. However, it was shown that antibodies could penetrate a significant distance into the VSG coat (Hsia et al., 1996) but not to the small plasma membrane proximal VSG domain (Schwede et al., 2011). Both the ligand size and the penetration of antibodies into the VSG coat made it unlikely that receptors were sterically protected from antibody binding. Immunization of mice with recombinant ISG65 or ISG75 did not protect against infection (Ziegelbauer & Overath, 1993). In addition, accessibility of the HpHbR was demonstrated by the ability of a monoclonal antibody drug conjugate to clear infections in a mouse model (MacGregor et al., 2019).

The trypanosome flagellar pocket is an invagination of the plasma membrane at the base of the single flagellum and is the sole site of endo- and exocytosis. The location of the flagellar

pocket at the posterior end of the cell is central to the mechanism of clearance of immunoglobulin molecules bound to VSG. The forward swimming motion of the trypanosome exerts a hydrodynamic force on the immunoglobulin that protrudes above the top of the VSG coat pushing the antibody-VSG complex towards the flagellar pocket and subsequent endocytosis (Engstler et al., 2007). Since the hydrodynamic flow requires only binding to a cell surface protein, it is likely to occur with any large ligand bound to a receptor providing it has free lateral movement in the plane of the membrane. The flagellar pocket is a discrete domain of the plasma membrane (Gadelha et al., 2009) with several exclusively localised proteins (Gadelha et al., 2015). At the neck of the pocket, there is a restriction introduced by close contact between the plasma membranes of the flagellum and pocket as it emerges onto the cell body. This flagellar pocket collar is maintained by specific proteins (Bonhivers et al., 2008)(Gadelha et al., 2009). The exclusive localisation of some proteins to the plasma membrane of the flagellar pocket, others to the cell body, and a range to both, indicates that there is regulated passage between the two domains of the plasma membrane.

There is variation in the reported localisation of receptors to different domains of the plasma membrane. TfR was the first receptor to be identified, it is glycosylphosphatidylinositol (GPI)-anchored and has been localised to the flagellar pocket and endosomal membrane in some studies but others suggested it was on the flagellar pocket, cell body plasma membrane and endosomal membrane (Duncan et al., 2024; Mussmann et al., 2003, 2004; Steverding et al., 1994a, 1995; Tiengwe et al., 2017). The Complement Factor H receptor (FHR) is a monomer probably GPI-anchored and is localised to the cell body and flagellar plasma membrane (Macleod et al., 2020). HpHbR, also probably GPI-anchored, has been localised to the flagellar pocket (Vanhollebeke et al., 2008). Reporter proteins with a single GPI-anchor are also present on the cell body plasma membrane (Schwartz et al. 2005). ISG65 and ISG75 are type I transmembrane proteins and localise to the flagellar, cell body, and pocket plasma membrane as well as the endosome (Leung et al., 2011; Ziegelbauer et al., 1992). The localisation of receptors to the flagellar pocket has been proposed to protect the cell from downstream effects of antibody recognition of the receptor but the discovery of new receptors, such as Complement C3 binding by ISG65 (Macleod et al., 2022) and FHR (Macleod et al., 2020) that are more abundant and distributed over the cell surface seems to contradict this argument.

Newly synthesised or recycled proteins are added to the plasma membrane at the flagellar pocket. Some proteins are retained in the flagellar pocket and have limited or no distribution over the cell surface (Billington et al., 2023). It is assumed that these proteins have a

retention and/or retrieval signal. For transmembrane proteins a signal could be in the cytoplasm. In contrast, GPI-anchored proteins have no cytoplasmic component and recognition must occur on the external face of the plasma membrane. Any signal for retention has to operate in a background of sequence variation in VSGs which makes short amino acid motifs unlikely. TfR is a heterodimer with the two subunits, ESAG6 and ESAG7, forming a single binding site for monomeric transferrin. ESAG6, but not ESAG7, has a GPI-anchor so the TfR is tethered to the plasma membrane by a single anchor in contrast to VSG dimers and trimers which have a GPI-anchor on each subunit. There is experimental evidence that the signal for TfR concentration in the flagellar pocket is the number of GPI-anchors per molecule, a single anchor leading to a greater retention, and more than one anchor ready to escape to the surface of the cell body (Schwartz et al., 2005; Tiengwe et al., 2017). These experiments manipulated the number of GPI-anchors on TfR, heterodimer with a single anchor on one subunit. Adding an anchor to the second subunit caused a change in localisation to the cell surface and endosome as judged by immunofluorescence. However, conditions that led to a few fold increase in expression of single GPI-anchored TfR, including transferrin shortage and growth at high cell density, resulted in the detection of TfR on the cell body surface (Mussmann et al., 2004). Whether the surface-localized TfR is functional remains unproven (Mussmann et al., 2004; Schwartz et al., 2005).

TfR is encoded by a dispersed gene family with ~15 TfR variants. The experiments here started with a chance observation that one of these encoded a receptor with two GPI-anchors while the others have a single anchor. This was exploited to investigate how the presence of one or two GPI-anchors affected function. We show that the second GPI-anchor has no effect on the kinetics of uptake, or processing of transferrin through the endosome. However, the second anchor resulted in ≥1.5-fold increase in steady state receptor levels. Further, transferrin uptake experiments provided evidence that TfR was present over the entire cell surface and this was supported by immunofluorescence experiments. An analysis of the localisation of two other putatively GPI-anchored proteins showed that all were present over the entire cell surface. These experiments demonstrate that the trypanosome expresses a set of receptors over the entire cell surface inferring that there are effective mechanisms to resist antibody mediated recognition of conserved cell surface proteins.

RESULTS

The BES7 VSG expression site encodes a transferrin receptor with two GPI-anchors

166 In *T. brucei*, the active VSG gene is transcribed from a bloodstream form expression site
167 (BES) that is telomere proximal. BESs contain up to 12 other co-transcribed expression site
168 associated genes (ESAGs) (Hertz-Fowler et al., 2008; Pays et al., 2001). TfRs are
169 heterodimers encoded by ESAG6 and ESAG7 (Chaudhri et al., 1994; Salmon et al., 1994a)
170 The ESAG6 and 7 subunits share around 80% amino acid identity although ESAG6 has an
171 additional 24 residues at the C-terminus preceding a GPI-anchor addition signal. Different
172 BESs encode variants of ESAG6 and 7 with 90% or more amino acid sequence identity
173 (Maier & Steverding, 2008; Trevor et al., 2019). In *T. brucei* Lister 427, the isolate used in
174 these experiments, there are 15 BESs (Barcons-Simon et al., 2023) and most were
175 sequenced and annotated after transformation associated recombination cloning of
176 telomeres (Hertz-Fowler et al., 2008). In the original annotation, BES7 stands out as it has
177 two copies of ESAG6 but apparently lacked ESAG7 and as such would not be able to make
178 a functional TfR. Here, a fresh analysis of the sequence was performed and indicated that
179 the first 'ESAG6' gene annotated in BES7 actually encoded an ESAG7 with a C-terminal
180 extension and a GPI-anchor typical of an ESAG6. In addition, there was a second ESAG6
181 gene (ESAG6.2) downstream of the annotated copy (ESAG6.1), the two copies encode
182 proteins with a single difference in 401 residues (M110->V). Phylogenetic analysis of ESAG6
183 and ESAG7 confirmed that a copy of ESAG7 is indeed present in BES7 along with a single
184 copy of ESAG6 (Figure 1A).
185
186 The origin of the GPI-anchor attachment signal in BES7 ESAG7 was investigated by
187 comparing the ESAG7 mRNA sequences from 13 different BESs. This showed that all the
188 ESAG7 genes contained residual coding sequences for GPI-anchor addition but a set of
189 small deletions between nucleotides 985 and 1068 in the ORF resulted in a frameshift
190 leading to a premature stop codon at the C-terminal end effectively removing the GPI-anchor
191 attachment sequence (Figure S1). A comparison of BES7 ESAG6 and 7 showed that the C-
192 terminal 120 amino acid sequences are identical and there was a clear prediction for a GPI-
193 anchor on both using NetGPI 1.1 (Gíslason et al., 2021) (Figure S2).
194
195 **Cellular TfR protein levels are determined by BES identity and the number of GPI-**
196 **anchors**
197
198 ESAG6 and 7 protein levels were examined by western blotting in cell lines expressing
199 VSGs and TfRs from three different BESs: BES3-VSG118, BES1-VSG221 and BES7-
200 VSG224 (Figure 1B). TfRs have several N-linked glycosylation sites and whole cell lysates
201 were treated with PNGaseF to simplify analysis. First, in BES7 cells there was a shift in the
202 apparent molecular weight of ESAG7 from ~30 kDa to ~38 kDa, which is consistent with the

203 addition of an additional 24 residues present in ESAG6 but not ESAG7 and a GPI-anchor
204 (Figure 1B), such a change in mobility on the addition of a GPI-anchor to ESAG7 has been
205 reported previously (Tiengwe et al., 2017). Second, the identity of the active BES affected
206 both ESAG6 and ESAG7 protein levels, there were increasing levels of expression: BES3 <
207 BES1 < BES7 (Figure 1B). Lastly, when the BES7 cell line was modified to exchange
208 VSG224 to VSG221 (see below), this had little effect on TfR expression, suggesting the BES
209 identity was the dominant determinant rather than the VSG type. The rabbit TfR antiserum
210 used was raised against the TfR from BES1 (Gerrits et al., 2002) and is the same as used in
211 most other studies (Mussmann et al., 2003; Tiengwe et al., 2017). The amino acid sequence
212 identity between BES2 TfR and BES1 TfR is >98% and BES7 TfR is >92% and it is unlikely
213 that the difference in TfR levels result from differential reactivity of the serum to different
214 TfRs. Support for the different levels of TfR expression was obtained when the levels of TfR
215 mRNAs were estimated in the BES3, BES1 and BES7 cell lines using RNAseq (Table S1).
216 The level of TfR mRNAs were expressed as a ratio (ESAG6+ESAG7):VSG and were
217 consistent with the differences seen in protein levels (BES3, 0.022 < BES1, 0.038 < BES7,
218 0.077).
219
220 We next investigated whether GPI-anchor number contributed to the variation in cellular TfR
221 levels by making a set of transgenic cell lines (Figure 2A). First, VSG224 in BES7 was
222 changed to VSG221. Next, the cell line expressing VSG221 from BES7 was modified to alter
223 the ESAG7 by exchanging the 3' end of the ORF with that from BES1 ESAG7 resulting in
224 the loss of the GPI-anchor signal. As a control, a second cell line in which the ESAG7 gene
225 retained the GPI-anchor addition sequence was made. Similar modifications were performed
226 on cells expressing VSG221 from BES1, cell lines expressing either BES1 ESAG7 modified
227 with the C-terminal GPI-anchor sequence from BES7 ESAG7 or the endogenous BES1
228 ESAG7 were made. The result was four cell lines: all expressed VSG221 from either BES1
229 or BES7 and TfR with or without a GPI-anchor on ESAG7.
230
231 The cell lines were characterised by western blotting of PNGaseF-treated whole cell lysates
232 (Figure 2B). The addition of a GPI-anchor signal sequence to ESAG7 resulted in an increase
233 in both ESAG6 and 7. To estimate this change, whole cell lysates were minimally separated
234 by SDS-PAGE to collapse the ESAG6 and 7 proteins into a single band prior to western
235 blotting. Relative quantitation was obtained using a titration curve of the highest TfR
236 expresser and normalised against SCD6 for loading (Figure 2C). Three biological replicates
237 were performed and the levels of both TfRs from BES1 is significantly lower ($p<0.01$), ~3.5
238 fold, compared to BES7, regardless of GPI-anchor number. The presence of a GPI-anchor
239 on ESAG7, leading to a double-anchored TfR, significantly increased ($p<0.05$) the

240 expression level by approximately 1.9-fold in BES1 and about 1.5-fold in BES7. This
241 provides strong evidence that the presence of a GPI-anchor on ESAG7 contributes to the
242 higher cellular expression level of TfR, which could result from increased protein stability,
243 reported for VSGs, (Bangs et al., 1986; Engstler et al., 2004) or a higher rate of turnover
244 and/or greater shedding of the single GPI-anchored TfR (Schwartz et al. 2005).
245
246 **Transferrin uptake kinetics are similar in cells expressing TfRs with either one or two**
247 **GPI-anchors**
248
249 To investigate whether anchor number influenced function, BES7-VSG221 cell lines
250 expressing single or double GPI-anchored TfR were used. It has already been shown that a
251 TfR with double GPI-anchors is functional (Tiengwe et al., 2017), here the kinetics of
252 transferrin binding and uptake by single and double GPI-anchor TfRs were compared. The
253 experimental approach was similar to that developed to characterise the binding and
254 endocytosis of VSG antibodies (Engstler et al., 2007). The medium used to culture
255 trypanosomes contained ~2.5 μM transferrin (Kakuta et al., 1997), Alexa 568 labelled bovine
256 holo-transferrin (Tf_{A568}) was added to cultures, without any other manipulation, to a final
257 concentration of 0.5 μM (so that 1 in 6 molecules of Tf In the medium is now fluorescent)
258 and cells were then fixed over a time course from 15 to 600 seconds and imaged by
259 epifluorescence microscopy (Figure 3A and S3A). The on rate for binding of Tf to TfR is very
260 rapid (4.5×10^5 $M^{-1}s^{-1}$ at pH 7.4 for BES1 TfR and bovine Tf) (Trevor et al., 2019) and
261 binding will occur to unoccupied receptor almost immediately. At 15 seconds there was
262 variation between individual cells with Tf_{A568} present on the flagellum, across the cell body
263 and the flagellar pocket in both cell lines. There was also variation at 60 seconds, Tf_{A568} was
264 present in the endosomal compartment of most cells, and the cell surface in some cells. At
265 600 seconds the Tf_{A568} was predominantly within the endosomal compartment. The variation
266 was also examined by quantifying the fluorescence from individual cells (Figure 3B), this
267 showed the range of variation and an increase in fluorescence between 15 and 60 seconds
268 followed by a decrease by 600 seconds. Fluorescence intensity was also determined across
269 transverse sections of the cell (Figure 3C), this showed some cells with internal signal and
270 others with two peaks consistent with a cell surface localisation. There was a stronger signal
271 from cells expressing TfR with two GPI-anchors, consistent with higher expression levels,
272 but no consistent differences in distribution were seen.
273
274 The same Tf_{A568} uptake assay was performed with the BES1-VSG221 cells expressing TfRs
275 with one or two GPI-anchors (Figure 3D and S3B). There was a reduced binding and uptake

276 of Tf_{A568} in BES1 cells compared to BES7 cells as might be expected given lower levels of
277 the receptor. Otherwise, the time course of uptake was similar: at 15 seconds Tf_{A568} was
278 present on the flagellum and cell body surface as well as the flagellar pocket in both cell
279 lines, at 60 seconds Tf_{A568} on the cell surface was reduced and some was now present in the
280 flagellar pocket and endosomal compartments, and by 600 seconds Tf_{A568} was substantially
281 within endosomal compartments. In both BES7 and BES1 cell lines, fluorescence distribution
282 patterns across the cells showed variability at 15 and 60 sec (Figure 3E-F), but appeared
283 more uniform at 600 sec.
284
285 Previous studies have shown that some TfRs do not bind canine transferrin (Mussmann et
286 al., 2003). Canine transferrin has 501/686 amino acid sequence identities with bovine
287 transferrin (Figure S4A) and it was used as a negative control in the same transferrin binding
288 and uptake assay above using BES7-VSG221 cells expressing TfR with either one or two
289 GPI-anchors (Figure S4B). No cell binding or uptake of canine Tf in either cell line was
290 observed. In addition, a competition assay for binding of fluorescent Tf was performed by
291 adding 5- or 10-fold excess of unlabelled Tf at the same time (Figure S4C). The signal from
292 labelled Tf was reduced by the competition indicating saturable binding, consistent with a
293 receptor mediated process. These findings provide evidence that the binding of bovine
294 transferrin to the cell surface is receptor dependent. An important point is that fluorescent Tf
295 was added to cells in culture without any other manipulation as preliminary experiments
296 indicated that centrifugation, washing and resuspension in medium led to a reduction in
297 cellular TfR for up to 2 hours (Figure S4D).
298
299 Together, these experiments support a model in which the TfR is present on the cell surface,
300 and endocytosis is a rapid process. The greater Tf binding and uptake in BES7 compared to
301 BES1 cells provides evidence that TfR abundance limits the amount of Tf endocytosed. The
302 number of GPI-anchors on the TfR has no obvious influence on Tf uptake but does affect
303 receptor levels.
304
305 The finding that Tf_{A568} was bound over the whole cell surface at early time points in the
306 uptake assays suggested a similar localisation for the TfR. This is not consistent with some
307 previous studies that found TfR and other GPI-anchored receptors sequestered in the
308 flagellar pocket (Duncan et al., 2024; Mussmann et al., 2004; Steverding et al., 1994a, 1995;
309 Tiengwe et al., 2017; Vanhollebeke et al., 2008) or that expression level determined
310 localisation (Mussmann et al., 2003). We went on to characterise the cellular localisation of
311 single and double GPI-anchored TfR along with two other GPI-anchored receptors.
312

313 **Localisation of the transferrin receptor by immunofluorescence**
314
315 Previous reports provided evidence that in BES1-VSG221 cells grown in the presence of
316 10% FBS, the cell surface TfR is located or concentrated within the flagellar pocket and
317 endosome, rather than dispersed on the cell body (Ligtenberg et al., 1994; Mussmann et al.,
318 2003; Salmon et al., 1994a; Tiengwe et al., 2017). In contrast, when cells are treated to
319 increase TfR expression by roughly three to fivefold, for example when grown to high density
320 or in canine serum, TfR localizes on the cell body (Mussmann et al., 2003). To resolve this
321 discrepancy, the localisation of the TfR was investigated using immunofluorescence. Based
322 on the transferrin uptake experiments, we reasoned that the localisation of the TfR would be
323 very dynamic and thus chose to fix the cells in culture without any centrifugation or washing,
324 this approach was supported by preliminary experiments comparing protocols (Figure S5A-
325 B) that showed both the composition of the fixative and absence of a washing step altered
326 the outcome.
327
328 Four cell lines, BES1-VSG221 and BES7-VSG221 cells each expressing TfR with one or two
329 GPI-anchors, were investigated. Fixative was added to cells in culture without any other
330 manipulations, the final concentrations were 4% formaldehyde and 0.2% glutaraldehyde and
331 TfR localisation was observed by immunofluorescence after settling cells on microscope
332 slides. Under these experimental conditions, the TfR in all four cell lines had a distribution
333 across the entire cell surface including the flagellar pocket and in internal compartments in
334 some cells (Figure 4A). Fluorescence intensity measurements across transverse sections of
335 both the BES7 1- and 2 GPI cells confirmed that TfR is indeed present on the surface of
336 some cells as seen by two peaks in fluorescence corresponding to the cell periphery in some
337 cells (Figure 4B). As in the Tf uptake experiments, the strength of signal as measured by
338 total fluorescence intensity from individual cells showed that TfR abundance varied between
339 individual cells in populations (Figure 4C and Figure S5C). These measurements also
340 showed that the presence of two GPI-anchors on TfR increased levels by about 1.5-fold
341 compared to the single anchored receptor and that there is a ~3.5-fold higher TfR
342 expression in BES7 compared to BES1 cells regardless of GPI-anchor number. These
343 measurements support the western blot quantitation (Figure 2) and also provide evidence
344 that the immunofluorescence signal does not contain a significant level of non-specific
345 background.
346
347 Structured Illumination Microscopy (SIM) was used to obtain more information on TfR
348 localisation in the same four cell lines as above (Figure 5). TfR was present on the cell
349 surface including the flagellar pocket, cell body and flagellum, and in the endosome (single

350 stack images) (Figure 5A). Three-dimensional reconstruction of the localization of TfR
351 confirmed that it is distributed across the cell surface and in endosomes (Figure 5B).
352
353 These experiments collectively provide strong evidence that TfR is indeed present on the *T.*
354 *brucei* cell surface under normal growth conditions and that the localization pattern is
355 independent of the presence or absence of a GPI-anchor in the ESAG7 subunit.
356
357 **Cell surface localisation is shared by two other GPI-anchored receptors**
358
359 The finding that TfR is distributed over the whole cell surface led to an investigation of other
360 receptors. Two were selected on the basis of being predicted to have one or more GPI-
361 anchors and a non-expressing negative control being available. The first was the
362 haptoglobin haemoglobin receptor (HpHbR) for which +/+ and -/- cell lines were used. The
363 structure of most of HpHbR is known and it is a monomer in solution but two or more
364 receptors can bind a single ligand (Higgins et al., 2013; Lane-Serff et al., 2014). HpHbR has
365 a low copy number, 300 to 400 per cell (Vanhollebeke et al., 2008) and, in the absence of a
366 suitable antibody, a ligand uptake assay was used. The second receptor analysed was the
367 complement factor H receptor (FHR), this was used after a fortuitous observation that
368 although it is not expressed when cells are grown in medium containing 10% foetal bovine
369 serum (Macleod et al., 2020), it is expressed at high levels when the same cells are grown in
370 medium with 10% rabbit serum replacing the foetal bovine serum. The structure of FHR is
371 known and it is a monomer with a single GPI-anchor (Macleod et al., 2020).
372
373 Alexa 568-labelled HpHb ($HpHb_{A568}$) was used in uptake assays with HpHbR +/+ and -/-
374 cells as for transferrin uptake (Figure 6A). There was binding of ligand to the cell surface by
375 15 seconds, uptake into the endosome by 60 seconds, and a location consistent with the
376 lysosome by 600 seconds. Binding and uptake were not detected in HpHbR -/- cells (Figure
377 6A). The kinetics of uptake were similar to those for transferrin. Presence of $HpHb_{A568}$ on the
378 cell surface was confirmed by the fluorescence signal measurement across the cells at 15
379 seconds, which showed two distinct peaks consistent with peripheral localisation for some
380 cells (Figure 6B), the noise in the quantification is due to the low copy number of the
381 receptor. Again, there was variability in binding and uptake of HpHb across the population
382 (Figure S6).
383
384 In trypanosomes cultured in medium containing 10% rabbit serum, expression of the FHR
385 was readily detected whereas in medium containing foetal bovine serum (FBS) it is not
386 (Figure 7A). Cells cultured with rabbit serum were used to determine the localisation of FHR

387 by immunofluorescence following the same procedure used for the transferrin receptor
388 (Figure 7B). The FHR was clearly localised over the entire cell surface. Two controls for
389 specificity of antibody binding were performed: first cells were grown in medium
390 supplemented with foetal bovine serum and second with a no primary antibody control for
391 the cells grown with rabbit serum to control for cell surface immunoglobulin originating from
392 the growth medium. Neither control gave a signal (Figure S7). SIM analysis further provided
393 spatial resolution along with reconfirming the distribution of the FHR across the trypanosome
394 cell surface and flagellum as well as within the flagellar pocket (Figure 7C).
395
396 These experiments show that the detection of TfR on the cell surface is part of a general
397 pattern where GPI-anchored receptors are distributed across the cell body plasma
398 membrane.
399
400 **DISCUSSION**
401
402 Any pathogen that has evolved to establish and maintain a long-term infection within a
403 mammalian host must be able to acquire nutrients as well as be resistant to both the innate
404 and adaptive immune responses of the host. African trypanosomes have evolved a strategy
405 that is dependent on variant surface glycoprotein (VSG), a superabundant protein that forms
406 a densely packed coat on the cell surface. Low frequency switching to a different VSG
407 allows the population to persist (Mugnier et al., 2015). The VSG coat appears to prevent
408 antibodies, and possibly innate immunity factors, gaining immediate access to the plasma
409 membrane (Schwede et al., 2011). However, such a coat cannot be totally impermeable as
410 trypanosomes require host macromolecules such as transferrin and haptoglobin-
411 haemoglobin which they acquire through receptor mediated endocytosis (Lane-Serff et al.,
412 2014; Salmon et al., 1994b; Steverding et al., 1994b, 1995; Trevor et al., 2019; Vanhollebeke
413 et al., 2008).
414
415 Why these receptors do not result in the trypanosomes becoming susceptible to immune
416 recognition and attack is central to understanding the mechanisms of infection (Banerjee et
417 al., 2024). One model proposed that the receptors are sequestered in the flagellar pocket, an
418 invagination of the plasma membrane at the base of the flagellum, and are not accessible to
419 immune effectors. The idea that sequestration in the flagellar pocket allowed receptors to
420 hide from host immune effectors was first challenged by the discovery of invariant surface
421 glycoproteins (ISGs) (Ziegelbauer et al., 1992; Ziegelbauer & Overath, 1992) that were
422 shown to be distributed over the whole cell surface (Macleod et al., 2022; Ziegelbauer &
423 Overath, 1993). Two ISGs were subsequently identified as receptors, one for complement

424 C3 and another for the Fc region of immunoglobulins (Macleod et al., 2022; Mikkelsen et al.,
425 2024). Both the ability to access ligands and the structures of the extracellular domains of
426 both ISGs indicated that they were unlikely to be physically shielded by the VSG coat. The
427 ISGs are type 1 transmembrane proteins with a large extracellular domain, a single
428 transmembrane pass and a small cytoplasmic tail. In contrast, VSGs have two or more GPI-
429 anchors whereas the two characterised nutrient receptors have a single GPI-anchor. Could
430 this difference in GPI-anchor number result in selective retention of nutrient receptors in the
431 flagellar pocket (Tiengwe et al., 2017) as it is difficult to envisage a requirement for any
432 amino acid sequence motifs in the context of variation of VSGs.
433
434 Here, we have investigated the distribution of GPI-anchored receptors on the cell surface of
435 mammalian infective *Trypanosoma brucei*. The main findings are: (1) The majority of TfRs
436 encoded in the genome have a single GPI-anchor but there is at least one with two GPI-
437 anchors. (2) The single anchored TfRs probably arose from loss of one anchor as opposed
438 to gain in the double anchored version. The loss of the GPI-anchor from ESAG7 may
439 provide a selective advantage possibly reducing exposure to the host adaptive immune
440 system without affecting transferrin acquisition (Trevor et al., 2019). (3) The steady state
441 level of TfR varies with the identity of the transcribed BES. (4) Single or double anchored
442 TfRs bind transferrin, as previously reported (Tiengwe et al., 2017) and result in similar
443 kinetics of transferrin uptake, with movement from the cell surface to the endosome
444 occurring within two minutes. The rapid kinetics of uptake indicates the receptor ligand
445 complex is probably subject to the same hydrodynamic forces as antibody VSG complexes
446 (Engstler et al., 2007) resulting in a directional movement towards the posterior end of the
447 cell, the location of the flagellar pocket and endocytosis. (5) Adding a second GPI-anchor to
448 a TfR resulted in a ~1.5-fold increase in cellular receptor levels. (6) Both single and double
449 GPI-anchored TfRs are present over the whole cell surface as seen by both transferrin and
450 antibody binding. (7) Two other GPI-anchored receptors, the HpHbR and FHR, both
451 probably with a single GPI-anchor, are present over the whole cell surface.
452
453 The earlier findings that the TfR, and subsequently the HpHbR, are localised to the flagellar
454 pocket is an attractive model as it provided an easy explanation for why the receptors did not
455 result in immune attack. The experiments presented here do not agree with this model and it
456 is worth discussing the reasons why these experimental differences have arisen. Here the
457 cells were fixed in culture using formaldehyde and a higher concentration (0.2%) of
458 glutaraldehyde than in previous reports. In contrast, much of the previous work involved
459 manipulations of the trypanosomes before determining either transferrin binding or TfR/
460 HpHbR localisation by immunofluorescence. The most common is centrifugation and

461 washing prior to fixation for immunofluorescence (Engstler et al., 2004; Roggy & Bangs,
462 1999; Tiengwe et al., 2017; Vanhollebeke et al., 2008), a process that is slow when
463 compared to the very rapid endocytosis of surface bound transferrin (Figure 3) and providing
464 time for the ligand bound receptors to be cleared from the cell surface. This would be even
465 more apparent if the experimental manipulation reduced the export of new or recycled TfRs
466 to the cell surface. An example of how protocols determine outcomes is the variation in the
467 measured half-life of TfR, which ranges from ~40 min to 7 hrs depending on the different
468 experimental protocols used (Biebinger et al., 2003; Kabiri & Steverding, 2000; Mussmann et
469 al., 2004; Tiengwe et al., 2017).
470
471 The experiments involving transferring BES1-VSG221 cells to medium in which FBS had
472 been replaced by canine serum (Mussmann et al., 2003) are informative. The BES1 TfR
473 does not bind canine transferrin and cell proliferation arrested. After ~5 days, proliferating
474 cells appeared in the culture having switched BES and thus TfR orthologue to one able to
475 bind canine transferrin (van Luenen et al., 2005). In addition, supplementing the canine
476 serum based medium with bovine transferrin prevented arrest of proliferation indicating that
477 it was due to lack of transferrin alone (Mussmann et al., 2004). In contrast to experiments
478 that wash cells into solutions that do not support growth, the transfer of BES1-VSG221 cells
479 to medium with canine serum starves the cells of just transferrin. On transfer from FBS to
480 canine serum, the TfR abundance increased 4 to 5-fold and the receptor was present all
481 over the cell surface (Mussmann et al., 2003). It is unlikely that the distribution of TfR on the
482 cell surface results from a retention system being overwhelmed given the variation in TfR
483 expression observed from different BESs (Figure 1) but is due to an absence of ligand-
484 mediated uptake. Different TfRs have a wide range of affinities for transferrins (K_D from as
485 low as 1.4 nM to >5 μM) (Trevor et al., 2019) and there will be an equilibrium with the
486 relative amounts of TfR on the cell body surface compared with the flagellar pocket and
487 internal structures that will vary with the identity of the TfR and the identity and concentration
488 of transferrin.
489
490 The experiments here were informed by the kinetics of rapid transferrin uptake (Figure 3 and
491 as an unpublished observation in (Mussmann et al., 2004) and we did not manipulate the
492 cells before ligand uptake experiments or prior to fixation for immunolocalization. The result
493 was clear evidence that TfR is expressed over the whole cell surface and is not restricted to
494 the flagellar pocket. This was reinforced by the localisation of the HpHbR and FHR, both of
495 which are monomeric (Lane-Serff et al., 2014; Macleod et al., 2020), contain a single GPI-
496 anchor, and are also present over the whole cell surface. We also observed variation in TfR
497 and HpHbR abundance between individual cells, as has been seen previously for TfR

498 (Duncan et al., 2024; Steverding et al., 1994b), and this suggests sensitivity to the
499 requirements at the individual cell level. Whether this relates to cell cycle stage or any
500 developmental progression remains to be investigated. The expression of the TfR is
501 sensitive to the availability of Fe^{3+} with a several fold increases in mRNA and protein induced
502 by iron chelators (Gilabert Carbajo et al., 2021). Growth in medium dependent on rabbit
503 serum resulted in high levels of expression of the FHR, this could result from a factor in
504 rabbit serum inducing expression or failure to bind ligand.
505
506 The findings here still leave the question of how the trypanosome avoids receptor antibody-
507 based clearance by the host immune system? Vaccination of mice with ISGs did not result in
508 any protection (Ziegelbauer & Overath, 1993), this shows that receptors do not have to be
509 sequestered in the flagellar pocket to avoid the host adaptive immune system. The effective
510 killing of trypanosomes by antibody-drug conjugates recognising the HpHbR shows that
511 receptors are accessible (MacGregor et al., 2019), as does inhibition of transferrin binding by
512 Fab fragments (Steverding et al., 1995). It is likely that a combination of processes results in
513 resistance to receptor antibody-mediated killing: first antibodies have to recognise parts of
514 the receptor that are accessible in the VSG coat, this will be affected by the structure of the
515 receptor and how much is occluded by ligand binding, a function of ligand concentrations,
516 host species and receptor K_D. Enough antibody has to be present on the cell surface for long
517 enough to elicit a response. Two factors affect this, first the copy number of the receptor,
518 ISGs are present at 50,000 to 70,000 per cell (Ziegelbauer et al., 1992) (<1% of VSG), TfR
519 at a few thousand, but variable (Steverding et al., 1995), and HpHbR at 300 to 400
520 (Vanhollebeke et al., 2008). Second, the half time of the receptor antibody complex on the
521 cell body plasma membrane will be short (Steverding et al., 1995) as the hydrodynamic
522 forces rapidly push VSG-antibody complexes toward the flagellar pocket and endocytosis
523 (Engstler et al., 2007). In summary, we provide evidence that GPI-anchored receptors in
524 trypanosomes are not sequestered in the flagellar pocket but are distributed across the cell
525 body and flagellum surface plasma membrane and this leads to re-evaluation of how
526 trypanosomes avoid receptor antibody mediated clearance.
527
528
529 **MATERIALS AND METHODS**
530
531 **Cell lines**
532 *T. brucei* Lister427 bloodstream form cell lines were used throughout expressing either
533 VSG221 (MiTat1.2) from BES1, VSG118 (MITat 1.5) from BES3 or VSG224 (MITat 1.3) from

534 BES7. BES7 expressing cells were as described in Hertz-Fowler *et al.* (Hertz-Fowler et al.,
535 2008) where BES1 and BES7 were tagged with Puromycin and G418 resistance genes
536 respectively. Cells were maintained in culture in HMI-11 medium (Hirumi & Hirumi, 1989).
537 For ligand-uptake assays and immunofluorescence cells were harvested in mid-log phase
538 (0.5-1x10^6 cells/ml). To allow further modification by (CRISPR)-associated gene 9 (Cas9)
539 gene editing, BES1 and BES7 expressing cell lines were first modified by transfection with a
540 construct containing Cas9 and T7 RNA polymerase transgenes (Beneke et al., 2017).
541 Antibiotic selection was used when appropriate. The primers used to generate the cell lines
542 are listed in Table S5.
543
544 **Constructs for ESAG7 +/- GPI attachment site**
545 Constructs are represented schematically in Figure 2A and described in brief below:
546 BES7 constructs:
547 The presence of a G418 resistance gene upstream of ESAG7 was utilised to generate the
548 required constructs from BES7 genomic DNA (Hertz-Fowler et al., 2008). A PacI-EcoRI PCR
549 fragment from the promoter to the G418 resistance gene start was annealed to an EcoRI-
550 PacI PCR fragment from the G418 stop codon through to the ESAG7 3' UTR. The resulting
551 EcoRI site was used to insert a blasticidin resistance open reading frame. The entire
552 construct was cloned into pGEM-T, allowing the required cassette to be excised by PacI for
553 transfection into BES7 cells expressing Cas9, alongside suitable sgRNAs to target the
554 BES7-ESAG7 region, designed by ChopChop (https://chopchop.cbu.uib.no/). This construct
555 contained the endogenous BES7 ESAG7 including its GPI anchor. To remove the GPI
556 anchor addition sequences and express an ESAG7 similar to those in the other Lister427
557 bloodstream expression sites, a SacI-BsrBI fragment was excised and replaced with the
558 corresponding fragment from BES1 ESAG7. This fragment was generated by RT-PCR from
559 RNA isolated from BES1 VSG221 cells using standard methods.
560 BES1 constructs:
561 A similar approach was used to make ESAG7 modifying constructs from BES1 exploiting a
562 puromycin resistance gene located between the promoter and the ESAG7 gene in the BES1
563 expression site (Hertz-Fowler et al., 2008). PacI-BstEII and BstEII-PacI PCR fragments were
564 generated from genomic DNA, ligated and cloned into pGEM-T. To generate BES1-ESAG7
565 with a GPI anchor from the BES1 expression site, the distal SacI-PacI fragment was
566 replaced by a PCR fragment encoding SacI-ESAG7 stop codon (blunt end) from BES7-
567 ESAG7 DNA and a BES1-ESAG7 3' UTR region from the BES1 site corresponding to the
568 BES7-ESAG7 stop codon (blunt end) to PacI. Constructs were linearised with PacI and
569 transfected with sgRNAs targeting the ESAG7 gene in either BES7 or BES1 and

570 electroporated into BES1 VSG221 cells expressing Cas9. BES7 modified cell lines were
571 selected with blasticidin and BES1 modified cell lines with puromycin.
572 Changing the VSG from 224 to 221:
573 BES7-VSG224 expression was switched to VSG221 by transfection of a linearised plasmid
574 fragment encoding VSG221, flanked by 5' and 3' VSG221 intergenic regions and a
575 downstream G418 resistance gene flanked by alpha-beta tubulin intergenic regions.
576 Sequences targeting the 5' and 3' UTRs of the endogenous VSG224 gene were generated
577 by PCR from BES7 (TAR153) DNA (a kind gift of Luísa Figueiredo) and cloned via KpnI/XhoI
578 and SpeI/SacI fragments upstream and downstream of the VSG221-blasticidin expression
579 cassette. G418 resistant clones were screened for binding to anti-VSG221 antibody through
580 immunofluorescence assays and confirmed by Western blot analysis.
581
582 **Protein gel electrophoresis and Western blotting**
583 Protein samples were prepared and analysed by SDS-PAGE and western blotting following
584 standard methods. Briefly, cells were harvested by centrifugation, washed in serum-free
585 HMI-9 and resuspended in Protein Sample Buffer (10% glycerol, 2% w/v SDS, 80 mM Tris-
586 HCl pH 6.8), at a concentration of $2x10^8$ cells/ml. Immobilon-P membrane (Millipore) was
587 used to retain the proteins. The primary antibodies used during western blotting are rabbit
588 anti-FHR (Macleod et al., 2020) and rabbit anti-TfR (a kind gift of Piet Borst). Polyclonal anti-
589 VSG221 and anti-SCD6 antibodies were generated from recombinant *E. coli* expressed
590 proteins, injected into rabbits by standard methods (Covalab). Secondary antibodies used
591 were Peroxidase-conjugated AffiniPure Goat Anti-Rabbit IgG (H+L) (Jackson
592 Immunoresearch) and Alexa Fluor 488-Donkey Anti-Rabbit IgG (H+L) (Invitrogen).
593 Membranes were blocked in Tris-buffered saline (TBS), 0.1% Tween20, 2% w/v Marvel dried
594 milk and probed in appropriate dilutions of primary and secondary antibodies. Washing steps
595 were performed with TBS, 0.1% Tween20 and blots were analysed on a BioRad ChemiDoc
596 system, ensuring signals remained below saturation limits. Quantitation of transferrin
597 receptor protein level was performed using Fiji-ImageJ software
598 (https://imagej.net/software/fiji/), with background subtraction and comparison with intensity
599 measurements taken from a protein dilution series from BES7 expressing cells.
600
601 **RNAseq**
602 mRNA was sequenced using Illumina paired-end sequencing technology by the Beijing
603 Genomics Institute. Raw reads were deposited to ENA under the accession number
604 PRJEB90063. Analysis was perfomed using Galaxy (www.usegalaxy.org) (Afgan et al.,
605 2018). Reads were quality filtered using Trimmomatic (Bolger et al., 2014). Sequences were
606 searched for all common Illumina adaptors and the settings used were: LEADING:10

607 TRAILING:10 SLIDINGWINDOW:5:15 MINLEN:50. mRNA abundance was calculated using
608 SalmonQuant with default settings and *Trypanosoma brucei* Lister strain 427 2018 v68
609 reference transcriptome and genomes from TriTrypDB (Aslett et al., 2010).
610
611 **Ligand uptake**
612 Bovine holo-transferrin (ThermoFisher) was dialyzed against PBS and labelled with Alexa
613 fluor 568 NHS ester (ThermoFisher) following the manufacturer's protocol. Canine
614 transferrin was obtained from Abbexa and loaded with iron using a four-fold molar excess of
615 ammonium iron (III) sulphate in presence of 5 mM sodium bicarbonate followed by dialysis
616 against 10 mM HEPES pH 7.4, 150 mM NaCl as described previously (Trevor et al.,
617 2019)(Trevor et al., 2019). Canine holo- transferrin was then labelled with Alexa fluor 568
618 NHS ester (ThermoFisher) as above. The Hp-Hb complex was purified as described (Lane-
619 Serff et al., 2014) and labelled with Alexa fluor 568 NHS ester (ThermoFisher) following the
620 manufacturer's protocol.
621
622 Mid log-phase cells (~ 6 x 10^5 /ml) were supplemented with 500 nM Alexa 568 labelled ligand
623 and incubated at 37°C. At time points, cells were fixed by the addition of 8% formaldehyde in
624 PBS to a final concentration 1% and incubated for 5 min. Cells were further washed with
625 PBS plus 1% BSA and DNA was stained with Hoechst 33258. Slides were prepared and
626 images were captured within next within the next 30 min using Zeiss Axio Imager.Z2 with
627 X100 objective. Samples in any one experiment were excited with the same intensity and
628 using the same exposure time. Images were processed using the ZEN Blue software.
629
630 **Immunofluorescence localisation and microscopy**
631 *T. brucei* cells were fixed in culture by the addition of one volume of 8% formaldehyde, 0.4%
632 glutaraldehyde (EM grade TAAB Laboratories Equipment Ltd.) in PBS for 10 min. After
633 fixation, cells were washed with serum free HMI-9 plus 1% bovine serum albumin (BSA)
634 twice and immobilized on poly-lysine coated slides for 1 hr. Immobilized cells were treated
635 with 0.1% triton X-100 (in PBS) for 5 min , washed with PBS and then incubated with PBS,
636 1% BSA for 10 min. Cells were incubated with the rabbit anti-TfR (1:50) or anti- FHR
637 (Macleod et al., 2020) (1:50) in PBS, 1% BSA for 1 hr, washed three times with PBS and
638 then with donkey anti- rabbit Alexa488 (1:800) in PBS, 1% BSA for 1 hr. Cells were washed
639 three times with PBS and the last wash contained 0.1 µg/ml Hoechst 33258 to stain DNA.
640 Cells were mounted with anti-fade and were visualized under Zeiss Axio Imager.Z2 with
641 X100 objective. In any one experiment, samples were illuminated with same exposure time,
642 intensity for respective excitation channels. All immunofluorescence experiments were
643 repeated three to six times with similar results. The images were processed with ZEN Blue

software by adjusting the brightness and contrast with the same changes being made to all images in any one experiment including the negative controls. Individual cells were manually outlined to define the whole-cell regions of interest (ROI), and background fluorescence was measured from cell-free regions within the same field using the ZEN Blue software and it was subtracted. For each condition, mean fluorescence intensity (arbitrary unit) was quantified from at least 50-100 cells across the repeated experiments. Mean fluorescence intensity was measured and background fluorescence intensity was subtracted. ImageJ software was used to measure the point fluorescence intensity of ligands and receptor antibodies by drawing a line perpendicular to the long axis of the cell, and the distribution profile against the distance was plotted. For 3D structured illumination, a Zeiss Elyra7 microscope with X63 objective was used in the Cambridge Advanced Imaging Centre. Slides were prepared as above and the processing of all images and the 3D reconstruction were performed with ZEN Blue software only by adjusting the brightness contrast. All raw and processed images are available at EMBL-EBI BioImage Archive accession S-BIAD2480.

660 **FIGURE LEGENDS**

661

662 **Figure 1. *T. brucei* transferrin receptor expressed from BES7 contains GPI-anchored**
663 **ESAG7.**

664 (A) Phylogenetic tree showing the relationship between ESAG6 and ESAG7 proteins from *T.*
665 *brucei* Lister 427 (Hertz-Fowler et al., 2008). The tree was assembled in Geneious Prime
666 (www.geneious.com) using an alignment by Muscle 5.1 followed by a neighbour joining tree
667 with 100 bootstraps and no outgroup on residues 1 to 332 of the alignment. BES7 ESAG 6.1
668 and 7 are shown in red.

669 (B) Variation in transferrin receptor expression in cell lines expressing VSGs from different
670 bloodstream form expression sites (BES). BES3-VSG118, BES1-VSG221, BES7-VSG224
671 cell lines are unmanipulated and the BES7-VSG221 was made after exchanging VSG224 for
672 VSG221 (see Figure 2A). Cell lysates were treated with PNGaseF and 2 x 10^6 cells
673 equivalents were loaded. Western blots were probed with anti-TfR, and then overprobed with
674 anti-VSG221. ESAG6 and ESAG7 plus GPI-anchor variants are indicated; BES3-VSG118
675 and BES1-VSG221 cell lysates contain ESAG7 without the GPI anchor. BES3-VSG118 and
676 BES7-VSG224 cell lysates did not show any VSG221. The presence of VSG221 protein
677 confirmed the switching of BES7 VSG224 to VSG221. Switching in VSG type did not affect
678 the expression pattern of native TfR (ESAG6/7 plus GPI) protein. Coomassie blue stained
679 SDS-PAGE gel to demonstrate loading of samples.

680

681 **Figure 2. The effect of BES identity and the number of GPI-anchors on the cellular TfR**
682 **levels.**

683 (A) Schematic illustrating the production of cell lines. For the addition and removal of ESAG7
684 GPI-anchor addition sequences, two constructs were used for each of BES1 and BES7. A
685 description of the construct is provided in the methods. For BES7, the same process was
686 used, one construct removing the GPI-anchor from ESAG7, the other leaving it intact. For
687 BES1, integration of one resulted in modification of ESAG7 to add a GPI-anchor, integration
688 of the second resulted in an unchanged ESAG7 polypeptide sequence. Restriction enzyme
689 sites used in cloning: P, PacI; E, EcoRI; S, SacI; Bs, BstEII and Bb, BsrBI. The VSG in
690 BES7-VSG224 cells was switched to VSG221 to remove any VSG-dependent variation. The
691 targeting construct conferred G418 resistance. (B) Transferrin receptor expression in the
692 following cell lines: BES7-VSG221 single (1-GPI) and double (2-GPI) GPI-anchored TfR and
693 BES1-VSG221 single and double GPI-anchored TfR. Cell lysates were treated with
694 PNGaseF and 2 x 10^6 cells equivalents were loaded per gel track. A western blot of the
695 samples was probed with anti-TfR then over probed with anti-VSG221 and anti-SCD6.
696 ESAG6 and ESAG7 plus GPI-anchor variants are indicated.

697 (C) TfR quantitation estimates from a minimum of three biological replicates of each cell line,
698 error bars display the standard deviation for each sample. Samples plus a dilution series
699 from BES7-221 were minimally separated by SDS-PAGE to compress TfR components to a
700 single band for analysis after western blotting, probed with anti-TfR and anti-SCD6. Donkey
701 anti-rabbit Alexa 488 was used as secondary antibody and band intensity was calculated by
702 ImageJ ensuring that signals taken for each reading were below saturation levels. Relative
703 quantitation was determined by mapping values to those obtained from a dilution series.
704 Measurements for SDC6 were used to normalise cell loading with the value for BES1-1GPI
705 anchor samples given an arbitrary value of 1. Statistical analysis was used a two-tailed
706 paired t-test, $**p \leq 0.01$; $*p \leq 0.05$.
707
708 **Figure 3. Transferrin endocytosis is rapid, in both single and double GPI-anchored**
709 **cells. Initial binding is to the cell surface and internalization is detected within 60 sec.**
710 Cultures of single (1-GPI) or double (2-GPI) GPI-anchored TfR expressing BES7-VSG221
711 and BES1-VSG221 cells were supplemented with 500 nM Alexa568 labelled holo- transferrin
712 (Tf_{A568}) and incubated for 15 sec, 60 sec or 600 sec and fixed by addition of formaldehyde for
713 5 min. Following washing with PBS containing 1% bovine serum albumin cells were
714 visualized under Zeiss Axio Imager.Z2 with X100 objective. Images in all these experimental
715 time points for both 1- and 2GPI TfR cells were captured with same intensity of excitation
716 and exposure time.
717 (A) Images showing the location of bound or endocytosed transferrin in representative cells
718 in populations and at time points as indicated. Scale bar is 5 µm. Images were processed
719 with ZEN Blue 3.4 software without any deconvolution. Larger numbers of cells are shown in
720 Supplementary Figure 3.
721 (B) The variation between individual cells in transferrin binding and uptake and endocytosis
722 shown by measurements of total fluorescence intensity of Tf_{A568} in BES7 VSG221 1- and 2-
723 GPI TfR cells at 15 sec, 60 sec and 600 sec. Measurements were obtained using Zen Blue
724 3.4 software and normalizing the background fluorescence (Table S2). Scatter plots of
725 measurements of individual cells are shown for 1-GPI (grey) and 2-GPI (purple) TfRs. The
726 average and standard deviation are shown for each cell line.
727 (C) Tf_{A568} fluorescence intensity distribution across transverse sections of randomly selected
728 cells was measured using ImageJ software. The plots are shown for both BES7 1- and 2-
729 GPI cell lines, showing the pattern of individual cells in different colours at 60 sec and 600
730 sec.
731 (D) (E) and (F) Same as (A) (B) and (C) but with BES1-VSG221 1- and 2GPI TfR expressing
732 cells and Table S3 corresponds to (E).
733

734 **Figure 4. Immunofluorescence localisation of single and double GPI-anchored**
735 **transferrin receptors to the entire plasma membrane.**
736 Cell lines expressing VSG221 and either 1- or 2-GPI TfR variants were fixed in culture with
737 final concentrations of 4% formaldehyde and 0.2% glutaraldehyde. Immunofluorescence
738 localisations were performed with rabbit anti-TfR followed by donkey anti-rabbit Alexa 488
739 (green). Cells were visualized using a Zeiss Axio Imager.Z2 with X100 objective. Images in
740 all these experimental sets were captured with same intensity of excitation and exposure
741 time.
742 (A) Localization in cell lines as indicated. Scale bar is 5 µm. Images were processed with
743 ZEN Blue 3.4 software. A larger number of cells is shown in Supp. Figure 5.
744 (B) Fluorescence distribution across transverse sections of the cells was measured using
745 ImageJ software. Plots are shown for both BES7-VSG221 TfR cell lines, each cell in a
746 different colour.
747 (C) Mean anti-TfR fluorescence intensity in individual cells of both BES1 VSG221 and BES7
748 VSG221 1- and 2-GPI TfR cell population was measured using ZEN Blue 3.4 and
749 normalized against the background fluorescence (Table S4). Bar diagram shows the
750 fluorescence intensity of either 1-GPI (grey) or 2-GPI (purple) TfR from individual cells. The
751 columns represent the average and the error bars show the standard deviation.
752
753 **Figure 5. Localization of single and double GPI-anchored transferrin receptors under**
754 **3D structured illumination microscope.**
755 Cells expressing either 1- or 2-GPI-anchored TfR were fixed in culture with final
756 concentrations of 4% formaldehyde and 0.2% glutaraldehyde. Immunofluorescence
757 localisation was performed with rabbit anti-TfR and donkey anti-rabbit Alexa 488. Cells were
758 visualized using a Zeiss Elyra7 microscope with X63 objective. Images in all these
759 experimental sets were captured with same intensity of excitation and exposure time. (A)
760 Localization of TfR in different cell lines as indicated. Scale bar is 5 µm.
761 (B) 3D projection generated using ZEN Blue 3.4 software example cells from the cell lines as
762 indicated. These images show the localization pattern of TfR on the cell surface as well as
763 within intracellular compartments. X-Y-Z axis is indicated. Scale bar 5 µm.
764
765 **Figure 6. Haptoglobin-haemoglobin endocytosis assay. Initial binding is to the cell**
766 **surface followed by rapid endocytosis.**
767 Cells were supplemented with 500 nM Alexa 568 labelled HpHb, incubated for 15 sec, 60
768 sec or 600 sec and fixed in culture with 1% formaldehyde. Following washing with PBS
769 containing 1% bovine serum albumin. Cells were visualized under Zeiss Axio Imager.Z2 with

770 x100 objective. Images in all these experimental time points were captured with same
771 excitation intensity and exposure time.
772 (A) Images showing the location of HpHb in +/+ and -/- cells at different time points in
773 representative cells as indicated. Images were processed with ZEN Blue 3.4 software. Scale
774 bar is 5 µm. A greater number of cells is shown in Supp. Figure 6.
775 (B) HpHb fluorescence intensity distribution over transverse section of cells at 15 sec
776 measured using ImageJ software. Individual cells are shown in different colours.
777
778 **Figure 7. The complement factor H receptor localises to the cell surface.**
779 The observation that abundant FHR expression occurred in cells grown in rabbit serum but
780 not in FBS supplemented medium was used to investigate its localisation.
781 (A) Western blot analysis of FHR expression in *T. brucei* EATRO1125 cells grown in medium
782 supplemented with either foetal bovine serum or rabbit serum. Cell lysates were not treated
783 with PNGaseF and $2x10^6$ cells equivalent were loaded. The blot was probed with rabbit anti-
784 FHR and then overprobed with anti-SCD6 for loading.
785 (B) Immunofluorescence determination of localisation of FHR in cell lines as indicated. Cells
786 were fixed in culture with final concentration of 4% formaldehyde and 0.2% glutaraldehyde.
787 Rabbit anti-FHR antibody was followed by donkey anti-rabbit Alexa 488 secondary antibody.
788 A set of cells grown in RbS, fixed similarly and stained only with secondary antibody was
789 used as a control for residual rabbit IgG from the growth medium and cells grown in FBS for
790 non-expressers. Cells were visualized using a Zeiss Axio Imager.Z2 with x100 objective.
791 Scale bar is 5 µm. A larger number of cells is shown in Supp. Figure 7
792 (C) Localisation of FHR by 3D structured illumination microscopy. Cells fixed as above were
793 visualised using a Zeiss Elyra7 with x63 objective. Images were processed with ZEN Blue
794 3.4 software. Two representative cells images showing FHR in white and merged panel with
795 DNA in blue. Scale bar is 5 µm.
796
797 **SUPPLEMENTARY FIGURE LEGENDS**
798
799 **Supp Figure 1. Relationship between ESAG7 variants.**
800 A. Clustal W alignment of the nucleotide sequences of ESAG7s showing the translation
801 termination codon in red. The sequence for GPI-addition is present in all genes but a series
802 of small deletions between nucleotides 980 and 1080 resulted in a frame shift and a new
803 stop codon that effectively removed the C-terminal ~50 residues from the open reading
804 frame.

805 B. Same alignment but just including ESAG7 from BES1 and BES7 showing the
806 conservation of the coding potential to the 3' side of the stop codon in BES1 ESAG7
807 indicating the shorter ESAG7 genes probably arose from a longer BES7-like variant.
808 Functional stop codons are in red.
809
810 **Supp Figure 2. Relationship between ESAG 6 and 7.**
811 Clustal W alignment of BES7 ESAG6 and 7 nascent polypeptide sequences. Predicted
812 processing sites are indicated by yellow highlighting. The N-terminal signal sequence
813 cleavage site was predicted using SignalP 6.0 and GPI-anchor addition sites by NetGPI 1.1
814 as detailed below the alignment.
815
816 **Supp Figure 3. Transferrin endocytosis is rapid, in both single and double GPI-**
817 **anchored cells. Initial binding is to the cell surface and internalization is detected**
818 **within 60 sec.**
819 Larger fields of cells from the experiments shown in Figure 3. Scale bar is 20 µm.
820
821 **Supp Figure 4. Controls for specificity of bovine transferrin binding to *T. brucei* BES7**
822 **VSG221 transferrin receptors.**
823 (A) Clustal W alignment of the polypeptide sequences of cow and dog transferrin.
824 (B) Cultures were supplemented with 500 nM Alexa568 labelled canine holo- transferrin and
825 incubated for 60 sec and fixed in culture by addition of formaldehyde to 1%. Following
826 washing with PBS containing 1% bovine serum albumin cells were visualized under Zeiss
827 Axio Imager.Z2 with x100 objective. Images for both BES7 VSG221 1- and 2-GPI TfR cells
828 were captured with same intensity of excitation and exposure time.
829 Images showing the absence of any bound or endocytosed canine transferrin in around forty
830 cells in population of both 1- and 2GPI TfR cells. Scale bar is 20 µm. Images were
831 processed ZEN Blue 3.4 software. (C) Cultures of single (1-GPI) GPI-anchored TfR
832 expressing BES7-VSG221 cells were supplemented with either 0.5 µM Tf_{A568} only, 2.5 µM
833 unlabelled Tf plus 0.5 µM Tf_{A568}, or 5 µM unlabelled Tf plus 0.5 µM Tf_{A568}, and incubated for
834 15 sec, then fixed by addition of formaldehyde for 5 min. DNA was stained with Hoechst.
835 Following washing with PBS containing 1% bovine serum albumin cells were visualized
836 under Zeiss Axio Imager.Z2 with X100 objective. Larger field views in all these experimental
837 sets were captured with same intensity of excitation and exposure time. (D) BES7 cells in
838 late logarithmic phase growth were counted by haemocytometer, harvested by centrifugation
839 and treated as follows: Left panel: Lane 1 (t=0 FBS): washed briefly in serum-free HMI-9 and
840 resuspended at 1 x 10^8 cells/ml in protein sample buffer; Lanes 2-5, washed briefly in serum-
841 free HMI-9 and resuspended at 1 x 10^6 cells/ml in HMI-9 + 10% FBS (Lanes 2 and 3) or

842 HMI-9 + 1% BSA (lanes 4 and 5) for a further 1 or 2 h prior to re-harvesting as described for
843 lane 1. Right hand panel contains half the samples used for the left side but treated with
844 PNGaseF prior to resuspension in protein sample buffer. 2 x 10^6 cells/lane were separated
845 by SDS-PAGE on 15% gels. Western blot analysis was performed with anti-TfR, anti-ISG65
846 and anti-SDC6 antibodies.
847
848 **Supp Figure 5. Immunofluorescence localisation of single and double GPI-anchored**
849 **transferrin receptors to the entire plasma membrane.**
850 (A) Different fixation protocols for the localisation of single GPI-anchored TfR expressed
851 from BES7. Cells were fixed in culture with final concentrations of either 4% formaldehyde
852 plus 0.2% glutaraldehyde, 4% formaldehyde, or washed with (1X PBS+ 1% BSA) then fixed
853 with 4% formaldehyde plus 0.2% glutaraldehyde. Immunofluorescence localisations were
854 performed with rabbit anti-TfR followed by donkey anti-rabbit Alexa 488 and DNA was
855 stained with Hoechst. A Zeiss Axio Imager.Z2 with X100 objective was used to visualise the
856 cells. Images in all these experimental sets were captured with same intensity of excitation
857 and exposure time. Scale bar is 5 µm. Images were processed with ZEN Blue 3.4 software.
858 (B) A larger number of cells is shown for Supp. Figure 5A. Scale bar is 20 µm.
859 (C) Larger fields of cells from the experiments shown in Figure 4. Scale bar is 20 µm.
860
861 **Supp Figure 6. Haptoglobin-haemoglobin endocytosis assay. Initial binding is to the**
862 **cell surface followed by rapid endocytosis.**
863 Larger fields of cells from the experiments shown in Figure 6. Scale bar is 20 µm.
864
865 **Supp Figure 7. The complement factor H receptor localises to the cell surface.**
866 Larger fields of cells from the experiments shown in Figure 7B. Scale bar is 20 µm.
867

868 **ACKNOWLEDGEMENTS**

869 We would like to thank: Luísa Figueiredo for the gift of the cell line expressing VSG224 from
870 BES7 and a BES7 TAR clone; Piet Borst for the transferrin receptor antibodies; Jay Bangs
871 for a lot of fun discussions (but no fish); and the Cambridge Advance Imaging Centre for
872 Super Resolution Microscopy.

873

874 **FUNDING**

875 MC and MH are Wellcome Investigators (MC, 217138/Z/19/Z; MH, 220797/Z/20/Z). Initial
876 funding for SB was from the Newton-Bhabha Fund.

References:

Afgan, E., Baker, D., Batut, B., van den Beek, M., Bouvier, D., Cech, M., Chilton, J., Clements, D., Coraor, N., Grüning, B. A., Guerler, A., Hillman-Jackson, J., Hiltemann, S., Jalili, V., Rasche, H., Soranzo, N., Goecks, J., Taylor, J., Nekrutenko, A., & Blankenberg, D. (2018). The Galaxy platform for accessible, reproducible and collaborative biomedical analyses: 2018 update. *Nucleic Acids Research*, *46*(W1), W537–W544. https://doi.org/10.1093/nar/gky379

Aslett, M., Aurrecoechea, C., Berriman, M., Brestelli, J., Brunk, B. P., Carrington, M., Depledge, D. P., Fischer, S., Gajria, B., Gao, X., Gardner, M. J., Gingle, A., Grant, G., Harb, O. S., Heiges, M., Hertz-Fowler, C., Houston, R., Innamorato, F., Iodice, J., … Wang, H. (2010). TriTrypDB: a functional genomic resource for the Trypanosomatidae. *Nucleic Acids Research*, *38*(Database issue), D457-62. https://doi.org/10.1093/nar/gkp851

Banerjee, S., Minshall, N., Webb, H., & Carrington, M. (2024). How are Trypanosoma brucei receptors protected from host antibody-mediated attack? *BioEssays : News and Reviews in Molecular, Cellular and Developmental Biology*, e2400053. https://doi.org/10.1002/bies.202400053

Bangs, J. D., Andrews, N. W., Hart, G. W., & Englund, P. T. (1986). Posttranslational modification and intracellular transport of a trypanosome variant surface glycoprotein. *The Journal of Cell Biology*, *103*(1), 255–263. https://doi.org/10.1083/jcb.103.1.255

Barcons-Simon, A., Carrington, M., & Siegel, T. N. (2023). Decoding the impact of nuclear organization on antigenic variation in parasites. *Nature Microbiology*, *8*(8), 1408–1418. https://doi.org/10.1038/s41564-023-01424-9

Beneke, T., Madden, R., Makin, L., Valli, J., Sunter, J., & Gluenz, E. (2017). A CRISPR Cas9 high-throughput genome editing toolkit for kinetoplastids. *Royal Society Open Science*, *4*(5), 170095. https://doi.org/10.1098/rsos.170095

Biebinger, S., Helfert, S., Steverding, D., Ansorge, I., & Clayton, C. (2003). Impaired dimerization and trafficking of ESAG6 lacking a glycosyl-phosphatidylinositol anchor. *Molecular and Biochemical Parasitology*, *132*(2), 93–96. https://doi.org/10.1016/j.molbiopara.2003.07.005

Billington, K., Halliday, C., Madden, R., Dyer, P., Barker, A. R., Moreira-Leite, F. F., Carrington, M., Vaughan, S., Hertz-Fowler, C., Dean, S., Sunter, J. D., Wheeler, R. J., & Gull, K. (2023). Genome-wide subcellular protein map for the flagellate parasite Trypanosoma brucei. *Nature Microbiology*, *8*(3), 533–547. https://doi.org/10.1038/s41564-022-01295-6

Bolger, A. M., Lohse, M., & Usadel, B. (2014). Trimmomatic: a flexible trimmer for Illumina sequence data. *Bioinformatics (Oxford, England)*, *30*(15), 2114–2120. https://doi.org/10.1093/bioinformatics/btu170

Bonhivers, M., Nowacki, S., Landrein, N., & Robinson, D. R. (2008). Biogenesis of the trypanosome endo-exocytotic organelle is cytoskeleton mediated. *PLoS Biology*, *6*(5), e105. https://doi.org/10.1371/journal.pbio.0060105

Chaudhri, M., Steverding, D., Kittelberger, D., Tjia, S., & Overath, P. (1994). Expression of a glycosylphosphatidylinositol-anchored Trypanosoma brucei transferrin-binding protein complex in insect cells. *Proceedings of the National Academy of Sciences of the United States of America*, *91*(14), 6443–6447. https://doi.org/10.1073/pnas.91.14.6443

Cook, A. D., Carrington, M., & Higgins, M. K. (2024). Molecular mechanism of complement inhibition by the trypanosome receptor ISG65. *ELife*, *12*. https://doi.org/10.7554/eLife.88960

Duncan, S. M., Carbajo, C. G., Nagar, R., Zhong, Q., Breen, C., Ferguson, M. A. J., & Tiengwe, C. (2024). Generation of a bloodstream form Trypanosoma brucei double glycosyltransferase null mutant competent in receptor-mediated endocytosis of transferrin. *PLoS Pathogens*, *20*(6), e1012333. https://doi.org/10.1371/journal.ppat.1012333

Engstler, M., Pfohl, T., Herminghaus, S., Boshart, M., Wiegertjes, G., Heddergott, N., & Overath, P. (2007). Hydrodynamic flow-mediated protein sorting on the cell surface of trypanosomes. *Cell*, *131*(3), 505–515. https://doi.org/10.1016/j.cell.2007.08.046

Engstler, M., Thilo, L., Weise, F., Grünfelder, C. G., Schwarz, H., Boshart, M., & Overath, P. (2004). Kinetics of endocytosis and recycling of the GPI-anchored variant surface glycoprotein in Trypanosoma brucei. *Journal of Cell Science*, *117*(Pt 7), 1105–1115. https://doi.org/10.1242/jcs.00938

Gadelha, C., Rothery, S., Morphew, M., McIntosh, J. R., Severs, N. J., & Gull, K. (2009). Membrane domains and flagellar pocket boundaries are influenced by the cytoskeleton in African trypanosomes. *Proceedings of the National Academy of Sciences of the United States of America*, *106*(41), 17425–17430. https://doi.org/10.1073/pnas.0909289106

Gadelha, C., Zhang, W., Chamberlain, J. W., Chait, B. T., Wickstead, B., & Field, M. C. (2015). Architecture of a Host-Parasite Interface: Complex Targeting Mechanisms Revealed Through Proteomics. *Molecular & Cellular Proteomics : MCP*, *14*(7), 1911–1926. https://doi.org/10.1074/mcp.M114.047647

Gerrits, H., Mussmann, R., Bitter, W., Kieft, R., & Borst, P. (2002). The physiological significance of transferrin receptor variations in Trypanosoma brucei. *Molecular and Biochemical Parasitology*, *119*(2), 237–247. https://doi.org/10.1016/s0166-6851(01)00417-0

Gilabert Carbajo, C., Cornell, L. J., Madbouly, Y., Lai, Z., Yates, P. A., Tinti, M., & Tiengwe, C. (2021). Novel aspects of iron homeostasis in pathogenic bloodstream form Trypanosoma brucei. *PLoS Pathogens*, *17*(6), e1009696. https://doi.org/10.1371/journal.ppat.1009696

Gíslason, M. H., Nielsen, H., Almagro Armenteros, J. J., & Johansen, A. R. (2021). Prediction of GPI-anchored proteins with pointer neural networks. *Current Research in Biotechnology*, *3*, 6–13. https://doi.org/10.1016/j.crbiot.2021.01.001

Hertz-Fowler, C., Figueiredo, L. M., Quail, M. A., Becker, M., Jackson, A., Bason, N., Brooks, K., Churcher, C., Fahkro, S., Goodhead, I., Heath, P., Kartvelishvili, M., Mungall, K., Harris, D., Hauser, H., Sanders, M., Saunders, D., Seeger, K., Sharp, S., … Berriman, M. (2008). Telomeric expression sites are highly conserved in Trypanosoma brucei. *PloS One*, *3*(10), e3527. https://doi.org/10.1371/journal.pone.0003527

963 Higgins, M. K., Tkachenko, O., Brown, A., Reed, J., Raper, J., & Carrington, M. (2013).
964 Structure of the trypanosome haptoglobin-hemoglobin receptor and implications for
965 nutrient uptake and innate immunity. *Proceedings of the National Academy of Sciences*
966 *of the United States of America*, *110*(5), 1905–1910.
967 https://doi.org/10.1073/pnas.1214943110

968 Hirumi, H., & Hirumi, K. (1989). Continuous cultivation of Trypanosoma brucei blood stream
969 forms in a medium containing a low concentration of serum protein without feeder cell
970 layers. *The Journal of Parasitology*, *75*(6), 985–989.

971 Hsia, R., Beals, T., & Boothroyd, J. C. (1996). Use of chimeric recombinant polypeptides to
972 analyse conformational, surface epitopes on trypanosome variant surface
973 glycoproteins. *Molecular Microbiology*, *19*(1), 53–63. https://doi.org/10.1046/j.1365-
974 2958.1996.351878.x

975 Kabiri, M., & Steverding, D. (2000). Studies on the recycling of the transferrin receptor in
976 Trypanosoma brucei using an inducible gene expression system. *European Journal of*
977 *Biochemistry*, *267*(11), 3309–3314. https://doi.org/10.1046/j.1432-1327.2000.01361.x

978 Kakuta, K., Orino, K., Yamamoto, S., & Watanabe, K. (1997). High levels of ferritin and its
979 iron in fetal bovine serum. *Comparative Biochemistry and Physiology. Part A,*
980 *Physiology*, *118*(1), 165–169. https://doi.org/10.1016/s0300-9629(96)00403-3

981 Lane-Serff, H., MacGregor, P., Lowe, E. D., Carrington, M., & Higgins, M. K. (2014).
982 Structural basis for ligand and innate immunity factor uptake by the trypanosome
983 haptoglobin-haemoglobin receptor. *ELife*, *3*, e05553.
984 https://doi.org/10.7554/eLife.05553

985 Lane-Serff, H., MacGregor, P., Peacock, L., Macleod, O. J., Kay, C., Gibson, W., Higgins, M.
986 K., & Carrington, M. (2016). Evolutionary diversification of the trypanosome
987 haptoglobin-haemoglobin receptor from an ancestral haemoglobin receptor. *ELife*, *5*.
988 https://doi.org/10.7554/eLife.13044

989 Leung, K. F., Riley, F. S., Carrington, M., & Field, M. C. (2011). Ubiquitylation and
990 developmental regulation of invariant surface protein expression in trypanosomes.
991 *Eukaryotic Cell*, *10*(7), 916–931. https://doi.org/10.1128/EC.05012-11

992 Ligtenberg, M. J., Bitter, W., Kieft, R., Steverding, D., Janssen, H., Calafat, J., & Borst, P.
993 (1994). Reconstitution of a surface transferrin binding complex in insect form
994 Trypanosoma brucei. *The EMBO Journal*, *13*(11), 2565–2573.
995 https://doi.org/10.1002/j.1460-2075.1994.tb06546.x

996 MacGregor, P., Gonzalez-Munoz, A. L., Jobe, F., Taylor, M. C., Rust, S., Sandercock, A. M.,
997 Macleod, O. J. S., Van Bocxlaer, K., Francisco, A. F., D'Hooge, F., Tiberghien, A., Barry,
998 C. S., Howard, P., Higgins, M. K., Vaughan, T. J., Minter, R., & Carrington, M. (2019). A
999 single dose of antibody-drug conjugate cures a stage 1 model of African
1000 trypanosomiasis. *PLoS Neglected Tropical Diseases*, *13*(5), e0007373.
1001 https://doi.org/10.1371/journal.pntd.0007373

1002 Macleod, O. J. S., Bart, J.-M., MacGregor, P., Peacock, L., Savill, N. J., Hester, S., Ravel, S.,
1003 Sunter, J. D., Trevor, C., Rust, S., Vaughan, T. J., Minter, R., Mohammed, S., Gibson,
1004 W., Taylor, M. C., Higgins, M. K., & Carrington, M. (2020). A receptor for the
1005 complement regulator factor H increases transmission of trypanosomes to tsetse flies.
1006 *Nature Communications*, *11*(1), 1326. https://doi.org/10.1038/s41467-020-15125-y

1007 Macleod, O. J. S., Cook, A. D., Webb, H., Crow, M., Burns, R., Redpath, M., Seisenberger,
1008 S., Trevor, C. E., Peacock, L., Schwede, A., Kimblin, N., Francisco, A. F., Pepperl, J.,
1009 Rust, S., Voorheis, P., Gibson, W., Taylor, M. C., Higgins, M. K., & Carrington, M.
1010 (2022). Invariant surface glycoprotein 65 of Trypanosoma brucei is a complement C3
1011 receptor. *Nature Communications*, *13*(1), 5085. https://doi.org/10.1038/s41467-022-
1012 32728-9

1013 Maier, A., & Steverding, D. (2008). Expression and purification of non-glycosylated
1014 Trypanosoma brucei transferrin receptor in insect cells. *Experimental Parasitology*,
1015 *120*(2), 205–207. https://doi.org/10.1016/j.exppara.2008.07.004

1016 Mikkelsen, J. H., Stødkilde, K., Jensen, M. P., Hansen, A. G., Wu, Q., Lorentzen, J.,
1017 Graversen, J. H., Andersen, G. R., Fenton, R. A., Etzerodt, A., Thiel, S., & Andersen, C.
1018 B. F. (2024). Trypanosoma brucei Invariant Surface Glycoprotein 75 Is an
1019 Immunoglobulin Fc Receptor Inhibiting Complement Activation and Antibody-Mediated
1020 Cellular Phagocytosis. *Journal of Immunology (Baltimore, Md. : 1950)*, *212*(8), 1334–
1021 1344. https://doi.org/10.4049/jimmunol.2300862

1022 Mugnier, M. R., Cross, G. A. M., & Papavasiliou, F. N. (2015). The in vivo dynamics of
1023 antigenic variation in Trypanosoma brucei. *Science (New York, N.Y.)*, *347*(6229), 1470–
1024 1473. https://doi.org/10.1126/science.aaa4502

1025 Mussmann, R., Engstler, M., Gerrits, H., Kieft, R., Toaldo, C. B., Onderwater, J., Koerten, H.,
1026 van Luenen, H. G. A. M., & Borst, P. (2004). Factors affecting the level and localization
1027 of the transferrin receptor in Trypanosoma brucei. *The Journal of Biological Chemistry*,
1028 *279*(39), 40690–40698. https://doi.org/10.1074/jbc.M404697200

1029 Mussmann, R., Janssen, H., Calafat, J., Engstler, M., Ansorge, I., Clayton, C., & Borst, P.
1030 (2003). The expression level determines the surface distribution of the transferrin
1031 receptor in Trypanosoma brucei. *Molecular Microbiology*, *47*(1), 23–35.
1032 https://doi.org/10.1046/j.1365-2958.2003.03245.x

1033 Pays, E., Lips, S., Nolan, D., Vanhamme, L., & Pérez-Morga, D. (2001). The VSG
1034 expression sites of Trypanosoma brucei: multipurpose tools for the adaptation of the
1035 parasite to mammalian hosts. *Molecular and Biochemical Parasitology*, *114*(1), 1–16.
1036 https://doi.org/10.1016/s0166-6851(01)00242-0

1037 Pinger, J., Nešić, D., Ali, L., Aresta-Branco, F., Lilic, M., Chowdhury, S., Kim, H.-S., Verdi, J.,
1038 Raper, J., Ferguson, M. A. J., Papavasiliou, F. N., & Stebbins, C. E. (2018). African
1039 trypanosomes evade immune clearance by O-glycosylation of the VSG surface coat.
1040 *Nature Microbiology*, *3*(8), 932–938. https://doi.org/10.1038/s41564-018-0187-6

1041 Redpath, M. B., Windle, H., Nolan, D., Pays, E., Voorheis, H. P., & Carrington, M. (2000).
1042 ESAG11, a new VSG expression site-associated gene from Trypanosoma brucei.
1043 *Molecular and Biochemical Parasitology*, *111*(1), 223–228.
1044 https://doi.org/10.1016/s0166-6851(00)00305-4

1045 Roggy, J. L., & Bangs, J. D. (1999). Molecular cloning and biochemical characterization of a
1046 VCP homolog in African trypanosomes. *Molecular and Biochemical Parasitology*, *98*(1),
1047 1–15. https://doi.org/10.1016/s0166-6851(98)00114-5

1048 Salmon, D., Geuskens, M., Hanocq, F., Hanocq-Quertier, J., Nolan, D., Ruben, L., & Pays,
1049 E. (1994a). A novel heterodimeric transferrin receptor encoded by a pair of VSG
1050 expression site-associated genes in T. brucei. *Cell*, *78*(1), 75–86.
1051 https://doi.org/10.1016/0092-8674(94)90574-6

1052 Salmon, D., Geuskens, M., Hanocq, F., Hanocq-Quertier, J., Nolan, D., Ruben, L., & Pays,
1053 E. (1994b). A novel heterodimeric transferrin receptor encoded by a pair of VSG
1054 expression site-associated genes in T. brucei. *Cell*, *78*(1), 75–86.
1055 https://doi.org/10.1016/0092-8674(94)90574-6

1056 Schwartz, K. J., Peck, R. F., Tazeh, N. N., & Bangs, J. D. (2005). GPI valence and the fate of
1057 secretory membrane proteins in African trypanosomes. *Journal of Cell Science*, *118*(Pt
1058 23), 5499–5511. https://doi.org/10.1242/jcs.02667

1059 Schwede, A., Jones, N., Engstler, M., & Carrington, M. (2011). The VSG C-terminal domain
1060 is inaccessible to antibodies on live trypanosomes. *Molecular and Biochemical*
1061 *Parasitology*, *175*(2), 201–204. https://doi.org/10.1016/j.molbiopara.2010.11.004

1062 Steverding, D., Stierhof, Y. D., Chaudhri, M., Ligtenberg, M., Schell, D., Beck-Sickinger, A.
1063 G., & Overath, P. (1994a). ESAG 6 and 7 products of Trypanosoma brucei form a
1064 transferrin binding protein complex. *European Journal of Cell Biology*, *64*(1), 78–87.

1065 Steverding, D., Stierhof, Y. D., Chaudhri, M., Ligtenberg, M., Schell, D., Beck-Sickinger, A.
1066 G., & Overath, P. (1994b). ESAG 6 and 7 products of Trypanosoma brucei form a
1067 transferrin binding protein complex. *European Journal of Cell Biology*, *64*(1), 78–87.

1068 Steverding, D., Stierhof, Y. D., Fuchs, H., Tauber, R., & Overath, P. (1995). Transferrin-
1069 binding protein complex is the receptor for transferrin uptake in Trypanosoma brucei.
1070 *The Journal of Cell Biology*, *131*(5), 1173–1182. https://doi.org/10.1083/jcb.131.5.1173

1071 Tiengwe, C., Bush, P. J., & Bangs, J. D. (2017). Controlling transferrin receptor trafficking
1072 with GPI-valence in bloodstream stage African trypanosomes. *PLoS Pathogens*, *13*(5),
1073 e1006366. https://doi.org/10.1371/journal.ppat.1006366

1074 Trevor, C. E., Gonzalez-Munoz, A. L., Macleod, O. J. S., Woodcock, P. G., Rust, S.,
1075 Vaughan, T. J., Garman, E. F., Minter, R., Carrington, M., & Higgins, M. K. (2019).
1076 Structure of the trypanosome transferrin receptor reveals mechanisms of ligand
1077 recognition and immune evasion. *Nature Microbiology*, *4*(12), 2074–2081.
1078 https://doi.org/10.1038/s41564-019-0589-0

1079 van Luenen, H. G. A. M., Kieft, R., Mussmann, R., Engstler, M., ter Riet, B., & Borst, P.
1080 (2005). Trypanosomes change their transferrin receptor expression to allow effective
1081 uptake of host transferrin. *Molecular Microbiology*, *58*(1), 151–165.
1082 https://doi.org/10.1111/j.1365-2958.2005.04831.x

1083 Vanhollebeke, B., De Muylder, G., Nielsen, M. J., Pays, A., Tebabi, P., Dieu, M., Raes, M.,
1084 Moestrup, S. K., & Pays, E. (2008). A haptoglobin-hemoglobin receptor conveys innate
1085 immunity to Trypanosoma brucei in humans. *Science (New York, N.Y.)*, *320*(5876),
1086 677–681. https://doi.org/10.1126/science.1156296

1087 Ziegelbauer, K., Multhaup, G., & Overath, P. (1992). Molecular characterization of two
1088 invariant surface glycoproteins specific for the bloodstream stage of Trypanosoma
1089 brucei. *The Journal of Biological Chemistry*, *267*(15), 10797–10803.

1090 Ziegelbauer, K., & Overath, P. (1992). Identification of invariant surface glycoproteins in the
1091 bloodstream stage of Trypanosoma brucei. *The Journal of Biological Chemistry*,
1092 *267*(15), 10791–10796.

1093 Ziegelbauer, K., & Overath, P. (1993). Organization of two invariant surface glycoproteins in
1094 the surface coat of Trypanosoma brucei. *Infection and Immunity*, *61*(11), 4540–4545.
1095 https://doi.org/10.1128/iai.61.11.4540-4545.1993

1096

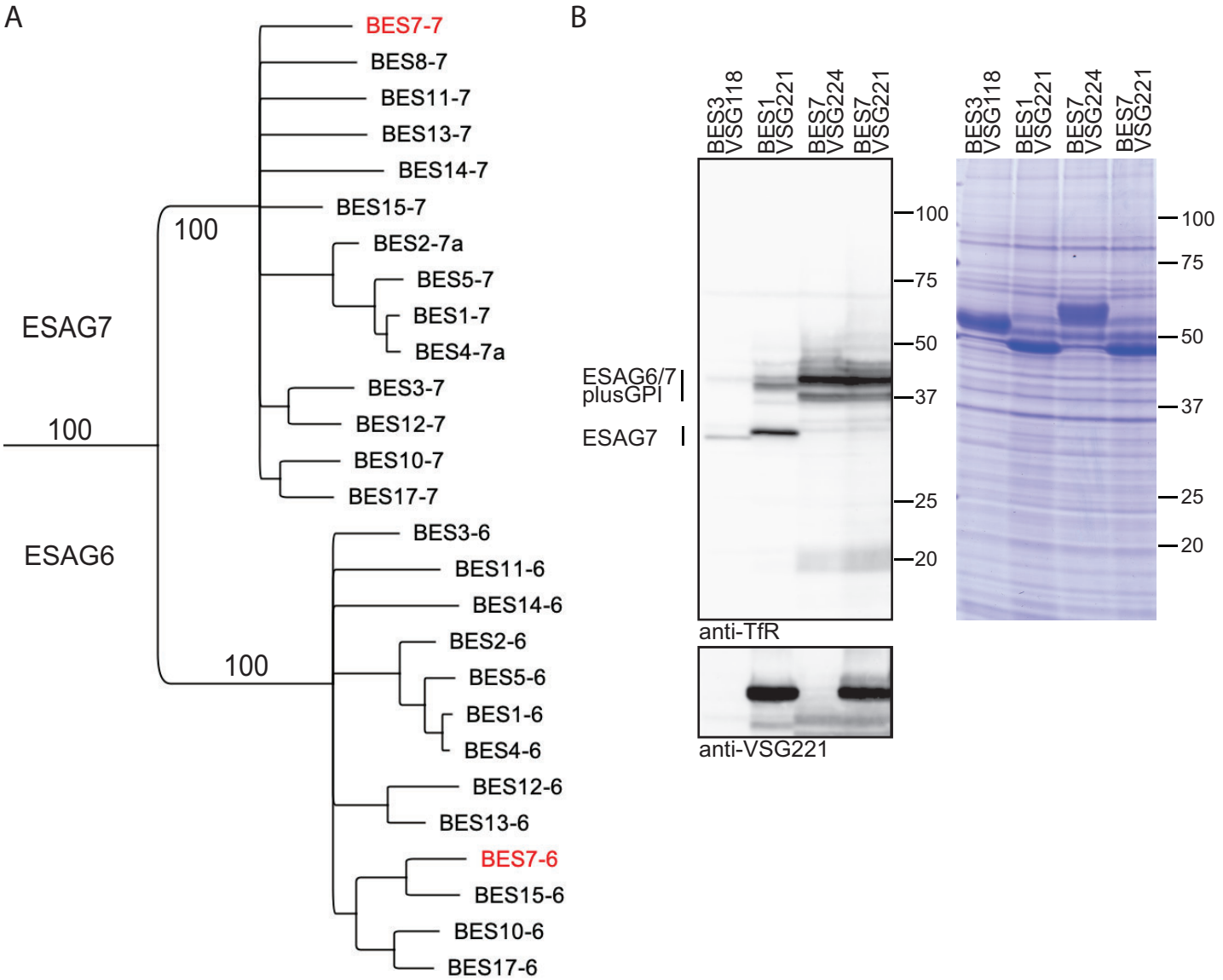
A
BES7-7
BES8-7
BES11-7
BES13-7
BES14-7
BES15-7
100
BES2-7a
BES5-7
BES1-7
BES4-7a
ESAG7
BES3-7
100
BES12-7
BES10-7
BES17-7
ESAG6
BES3-6
BES11-6
BES14-6
BES2-6
100
BES5-6
BES1-6
BES4-6
BES12-6
BES13-6
BES7-6
BES15-6
BES10-6
BES17-6
B
BES3 VSG118
BES1 VSG221
BES7 VSG224
BES7 VSG221
ESAG6/7 plusGPI
ESAG7
100
75
50
37
25
20
anti-TfR
anti-VSG221
BES3 VSG118
BES1 VSG221
BES7 VSG224
BES7 VSG221
100
75
50
37
25
20

Figure 1

A

Changes to BES7 ESAG7

altered anchor construct

ESAG6/7 genomic locus

unchanged anchor construct

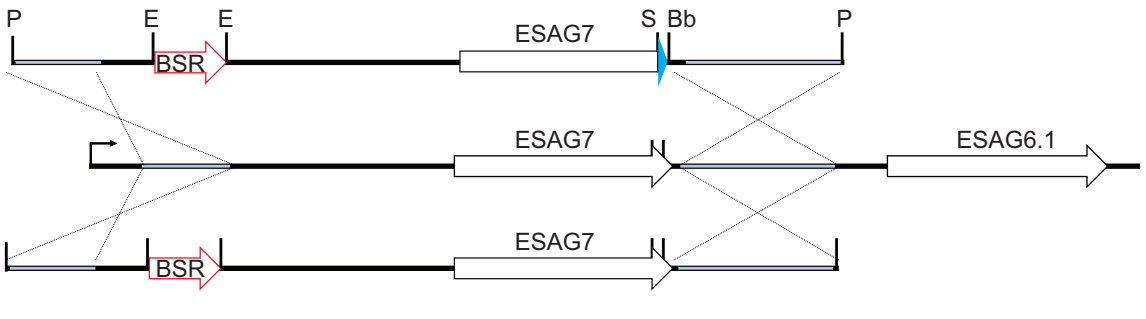

Changes to BES1 ESAG7

altered anchor construct

ESAG6/7 genomic locus

unchanged anchor construct

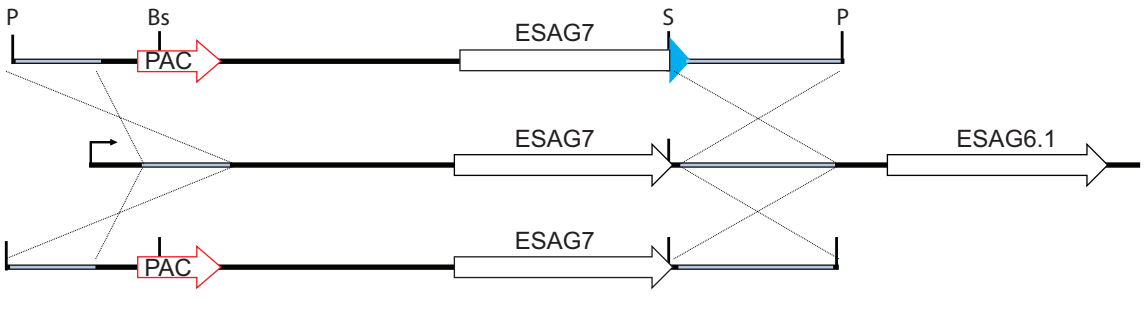

Changing BES7-VSG224 to BES7-VSG221

VSG224 genomic locus

replacement construct

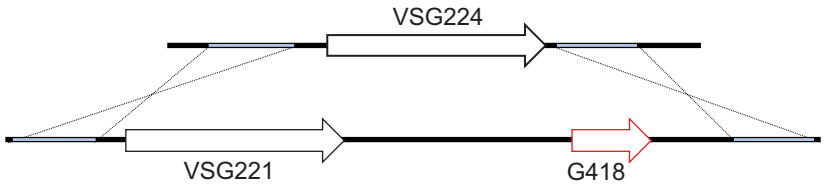

B

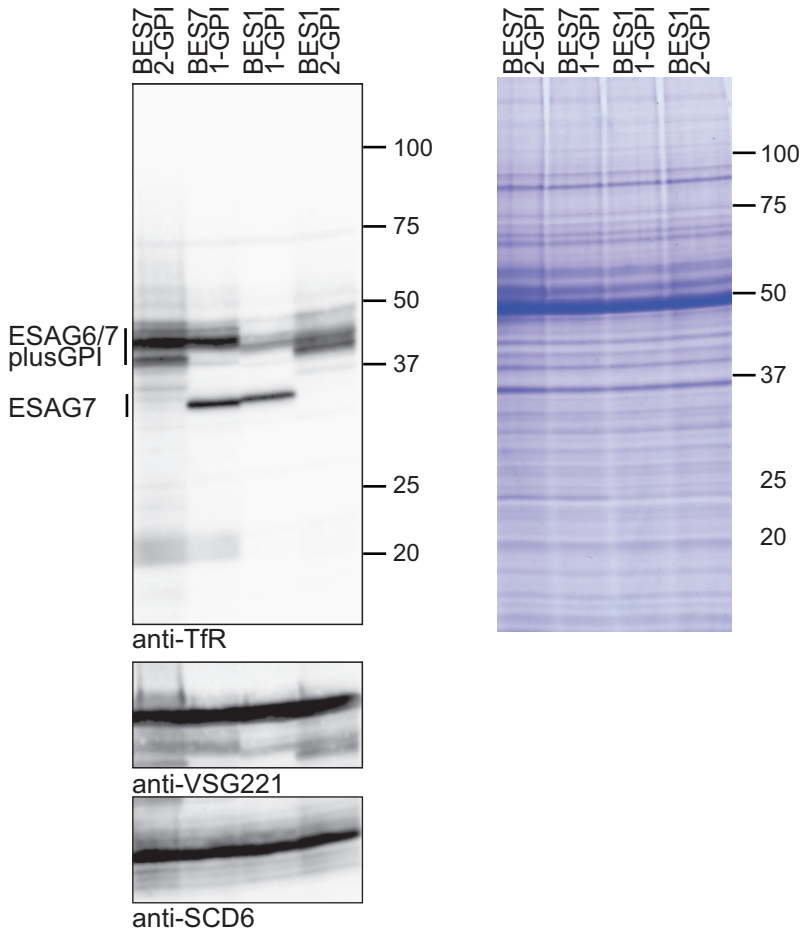

C

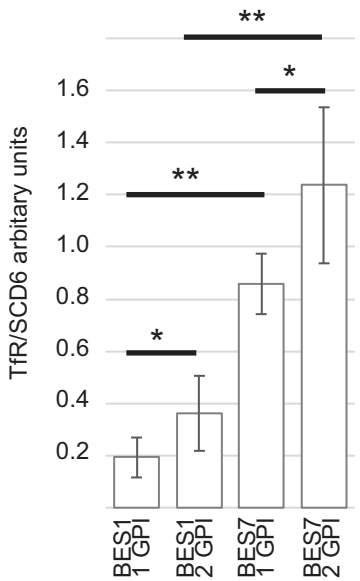

Figure 2

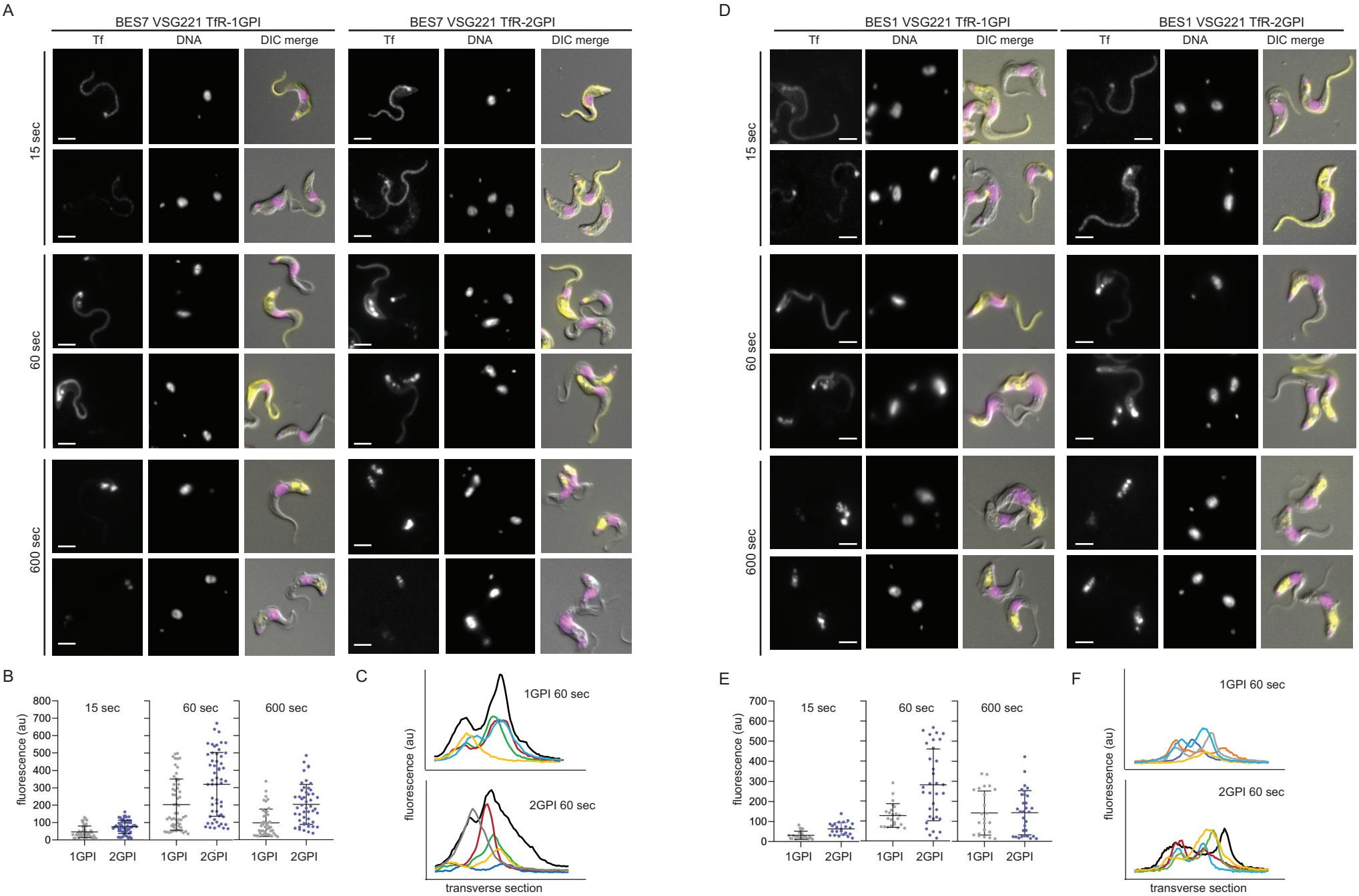
A
BES7 VSG221 TfR-1GPI
BES7 VSG221 TfR-2GPI
Tf
DNA
DIC merge
15 sec
60 sec
600 sec
D
BES1 VSG221 TfR-1GPI
BES1 VSG221 TfR-2GPI
B
fluorescence (au)
15 sec
60 sec
600 sec
1GPI
2GPI
C
1GPI 60 sec
2GPI 60 sec
transverse section
E
F

Figure 3

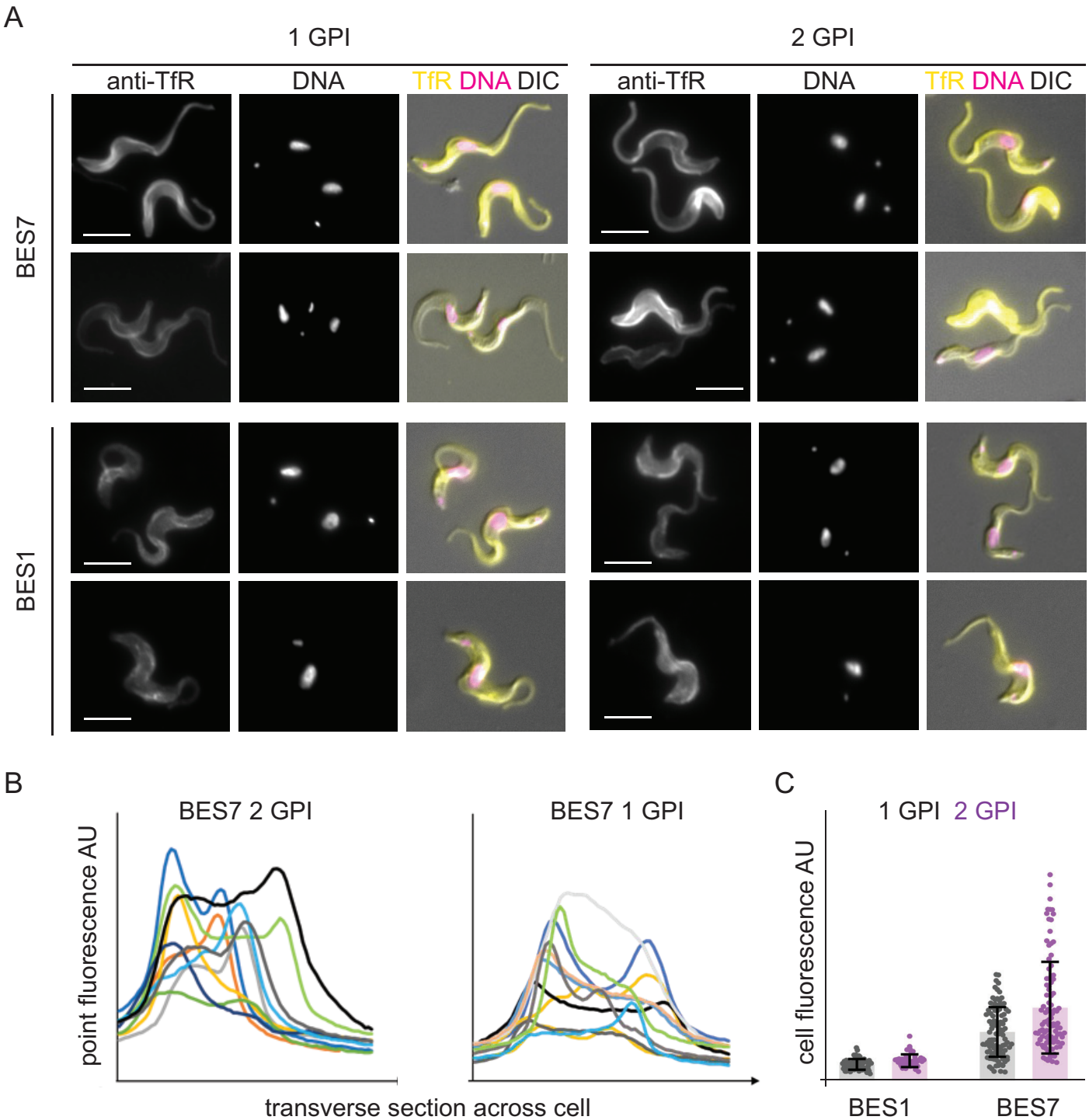
A
1 GPI
2 GPI
anti-TfR
DNA
TfR DNA DIC
anti-TfR
DNA
TfR DNA DIC
BES7
BES1
B
BES7 2 GPI
BES7 1 GPI
point fluorescence AU
transverse section across cell
C
1 GPI 2 GPI
cell fluorescence AU
BES1
BES7

Figure 4

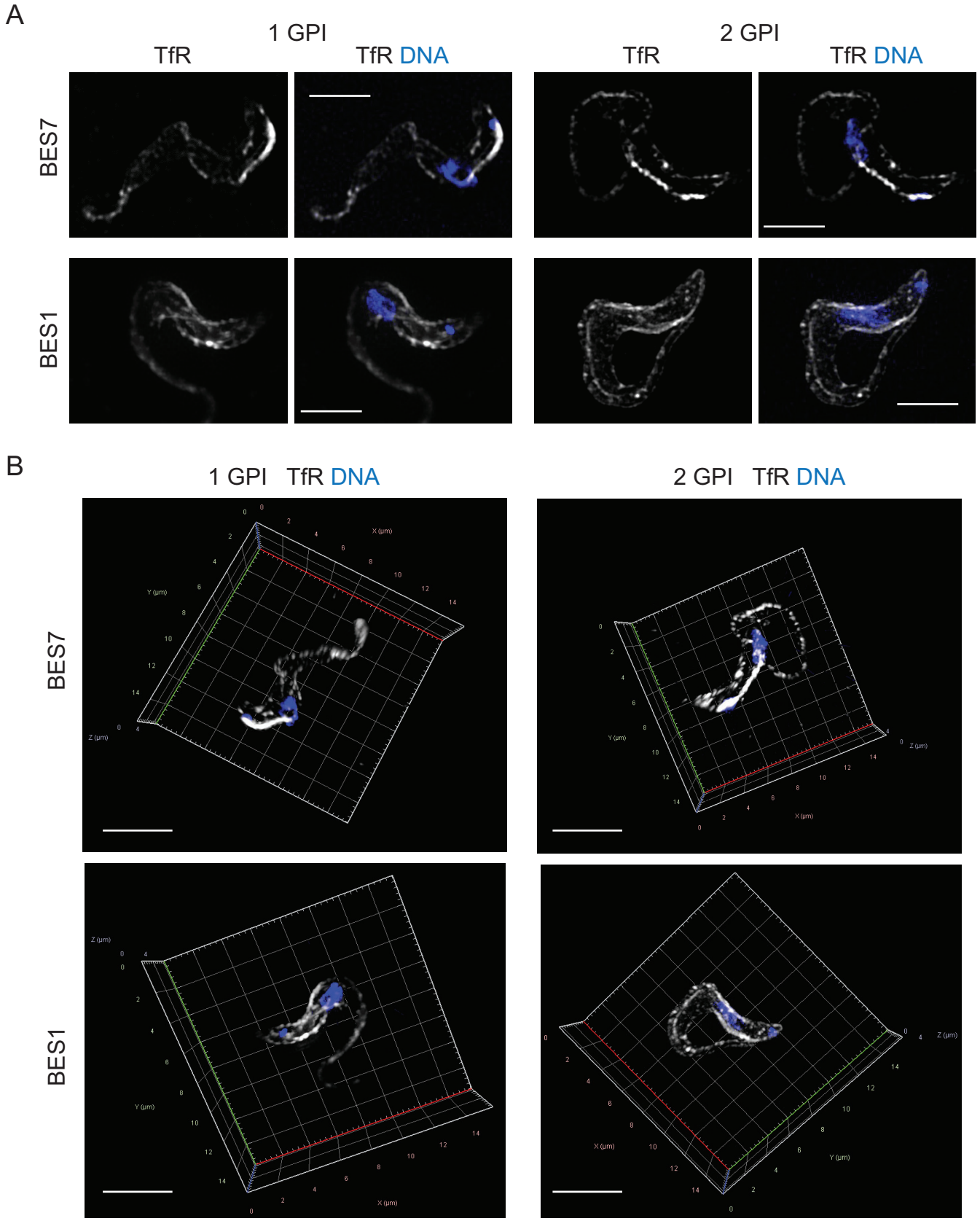
A
1 GPI
2 GPI
TfR
TfR DNA
TfR
TfR DNA
BES7
BES1
B
1 GPI TfR DNA
2 GPI TfR DNA
BES7
BES1

Figure 5

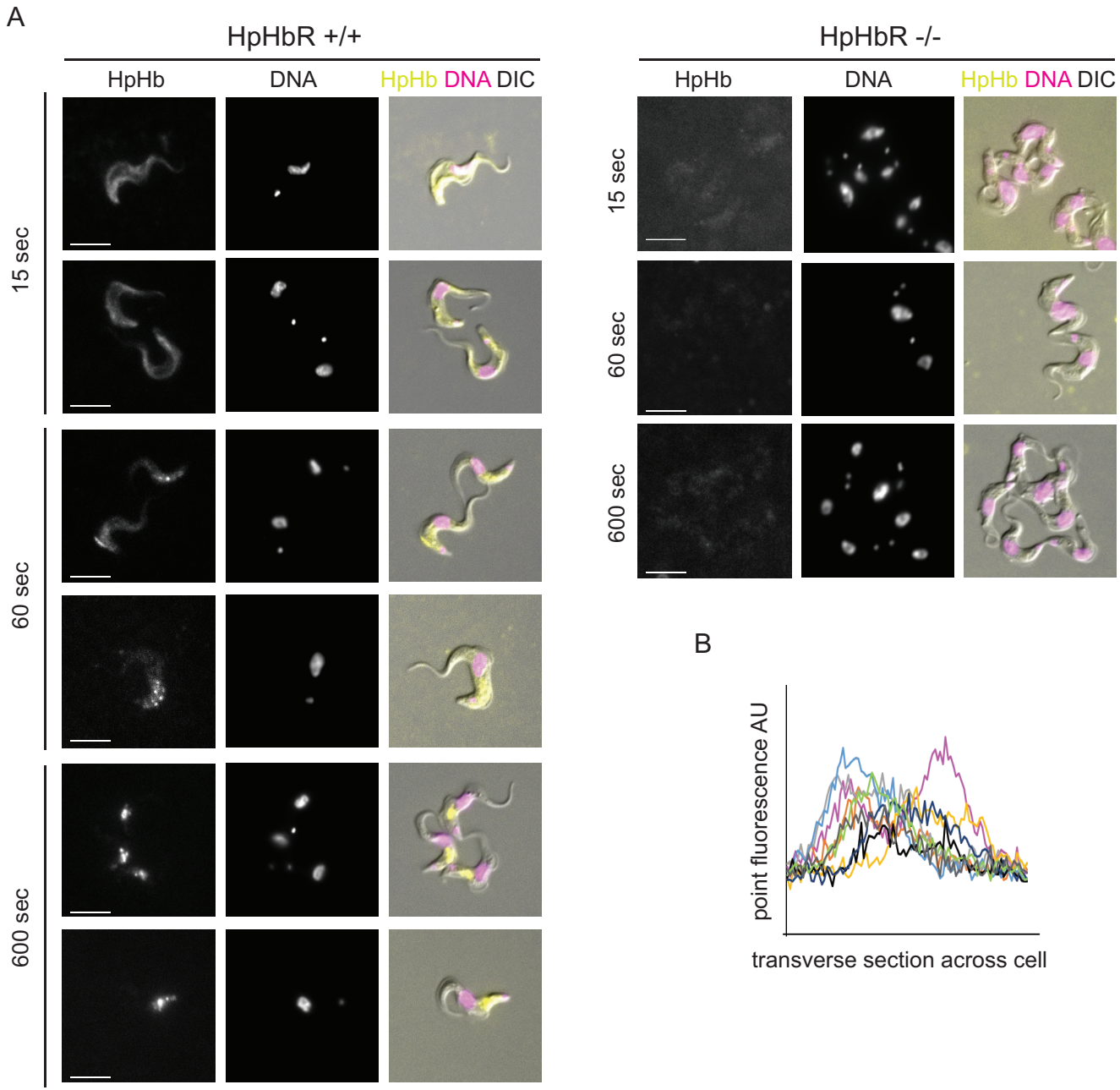
A
HpHbR +/+
HpHbR -/-
HpHb
DNA
HpHb DNA DIC
15 sec
60 sec
600 sec
B
point fluorescence AU
transverse section across cell

Figure 6

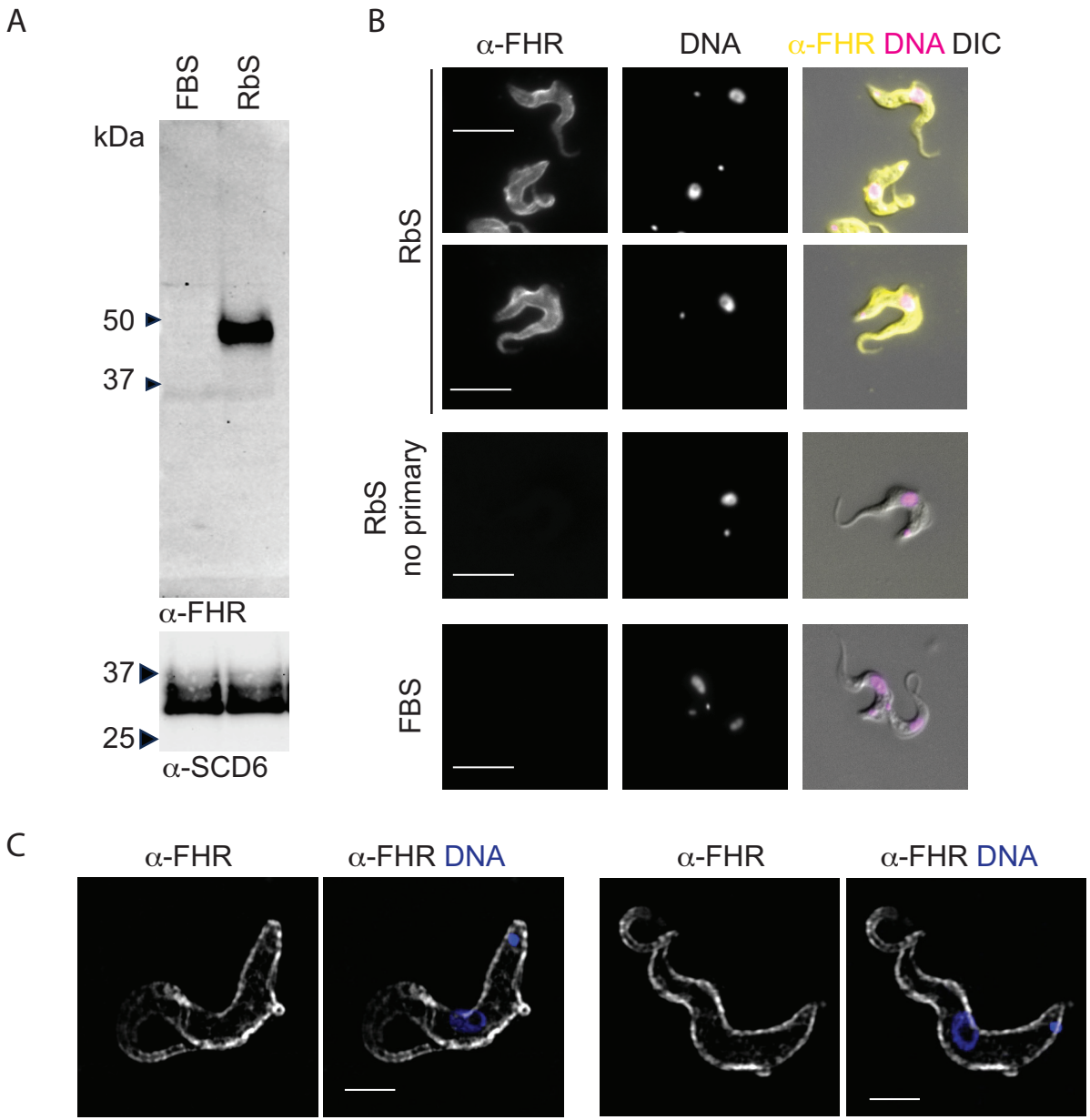
A
FBS
RbS
kDa
50
37
α-FHR
37
25
α-SCD6
B
α-FHR
DNA
α-FHR DNA DIC
RbS
RbS
no primary
FBS
C
α-FHR
α-FHR DNA
α-FHR
α-FHR DNA

Figure 7

A

ESAG7 ORFs from ~base 840

```
BES11    TTTAAGGATGTCATTCGCCTGTTTGCGCGCTTCAAAGAAGCAAAAAATGCAGTGATGAAGAAAATAAAAACTACTGTGGATGAATTGACTAAATGCATAGGGCAGAAAGAGGCTGAGCTC
BES2     TTTAAGGATGTCATCCGCCTGTTTGCGCGCTTCCAAGAAGCAAAAAATGCAGTGATGAATAAAATAAAAACTACTGTGGATGAATTGGCGAAATGCATAGGGCAGAAAGAGGTTGAGCTC
BES1     TTTAAGGATGTCATCCGCCTGTTTGCGCGCTTCCAAGAAGCAAAAAATGCAGTGATGAATAAAATAAAAACTACTGTGGATGAATTGGCGAAATGCATAGGGCAGAAAGAGGTTGAGCTC
BES4     TTTAAGGATGTCATTCGCCTGTTTGCGCGCTTCCAAGAAGCAAAAAATGCAGTGATGAATAAAATAAAAACTACTGTGGATGAATTGGCGAAATGCATAGGGCAGAAAGAGGTTGAGCTC
BES5     TTTAAGGATGTCATTCGCCTGTTTGCGCGCTTCCAAGAAGCAAAAAATGCAGTGATGAATAAAATAAAAACTACTGTGGATGAATTGGCGAAATGCATAGGGCAGAAAGAGGTTGAGCTC
BES7     TTTAAGGATGTCATTCGCCTGTTTGCGCGCTTCCAAGAAGCAAAAAATGCAGTGATGACGAAAATAAAAACTACTGTGGATGAATTGACGAAATGCATAGGGCAGAAGGAGGCTGAGCTC
BES13    TTTAAGGATGTCATTCGCCTGTTTGCGCGCTTCCAAGAAGCAAAAAATGCAGTGATGAGGAGAATAAAAACTACTGTGGATGAATTGACGAAATGTATAGGGAAGAAGGAGGCTGAACTC
BES14    TTTAAGGATGTCATTCGCCTGTTTGCGCGGTTCCAAGAAGCAAAAAATGAAGTGATGAATAAAATAAAAACTACTGTGGATGAATTGGCGAAATGCATAGGGCAGAAAGAGGTTGAGCTC
BES15    TTTAAGGATGTCATTCGCCTGTTTGCGCGGTTCCAAGAAGCAAAAAATGCAGTGATGACGAAAATAAAAACTACTGTGGATGAATTGACGAAATGCATAGGGCAGAAGGAGGCTGAACTC
BES12    TTTAAGGATGTCATTCGACTGTTTGCGCGCTTCCAAGAAGCAAAAAATGCAGTGATGAAGAAAATAAAAACTACTGTGGATGAATTGACGAAATGCATAGGGCAGAAAGAGGCTGAGCTC
BES3     TTTAAGGATGTCATTCGCCTGTTTGCGCGCTTCCAAGAAGTAAAAAATGCAGTGATGAAGAAAATAAAAACTACTGTGGATGAATTGACGAAATGCATAGGGCAGAAAGAGGCTGAGCTC
BES10    TTTAAGGATGTCATTCGCCTGTTTGCGCGCTTCCAAGAAGCAAAAAATGCAGTGATGAAGAAAATAAAAACTACTGTGGATGAATTGACGAAATGCATAGGGCAGAAGGAGGCTGAACTC
BES17    TTTAAGGATGTCATTCGCCTGTTTGCGCGCTTCCAAGAAGTAAAAAATGCAGTGGTGAAGAAAATAAAAACTACTGTGGATGAATTGACGAAATGCATAGGGCAGAAAGAGGCTGAGCTC
         ************** ** *********** *** ****** ******** **** ***  * ************************* * ***** ****** **** **** *** ***

BES11    ACTAATGATCAGCTTTACGAGGAATTT------GAGGCAATA----------------CAAAAGTATCTAGG-----------TTTTGGTAAAATGGAGTAAAAGC-----AAATTCAAC
BES2     ACTAATGATCAGCTTTACGAGGAATTC------GAGGCAATA----------------CAAAAGTACCTAGGG----------TCTCTGTGAAATGGAGTAAAAGC-----GAATTCAAC
BES1     ACTAATGATCAGCTTTACGAAGAATTC------GAGGCAATA----------------CAAAAGTACCTAGGG----------TCTCTGTGAAATGGAGTAAAGGC-----GAATTCAAC
BES4     ACTAATGATCAGCTTTACGAGGAATTC------GAGGCAATA----------------CAAAAGTACCTAGGG----------TCTCTGTGAAATGGAGTAAAAGC-----GAATTCAAC
BES5     ACTAATGATCAGCTTTACGAGGAATTC------GAGGCAATA----------------CAAAAGTACCTAGGG----------TCTCTGTGAAATGGAGTAAAAGC-----TAATTCAAC
BES7     ACTAATGATCAGCTTTACGAGGAATTTATCTGGGAGACCATAAACAGATTGGAGCTGTCAAAGAGAGTGAGTGAACAACCCTCTTTAGGTGAAGAAGAGGAGACGATCCTGAAATCTAAC
BES13    ACTAATGATCAGATTTACGAGGAATTC------GAGGCAATA----------------CAAAAGTATCTAGGG----------TTTCTGTGAAATGGAGTAAAAGC-----GAATCTAAC
BES14    ACTGATGATCAGCTTTACGAGGAATTC------GAGGCAATA----------------CAAAAGTATCTAGGG----------TTTCTGTGAAATGAAGTAAAAGC-----GAATCTAAC
BES15    ACTAATGATCAGATTTACGAGGAATTC------GAGGCAATA----------------CAAAAGTATCTAGGG----------TTTCTGTGAAATGGAGTAAAAGC-----GAATTTAAC
BES12    ACTAATGATCAGCTTTACGAGGAATTT------GAGGCAATA----------------CAAAAGTATCTAGGG----------TTTCTGTGAAATGGAGTAAAAGC-----GAATTTAAC
BES3     ACTAATGATCAGCTTTACGAGGAATTT------GAGGCAATA----------------CAAAAGTATCTATGG----------TTTCTGTGAAATGGAGTAAAAAC-----GAATCTAAC
BES10    ACTAATGATCAGATTTACGAGGAATTC------GAGGCAATA----------------CAAAAGTATCTAGGG----------TTTCTGTGAAATGGAGTAAAATC-----GAATCTAAC
BES17    ACTAATGATCAGCTTTACGAGGAATTT------GAGGTAATA----------------CAAAAGTATCTATGG----------TTTCTGTGAAATGGAGTAAAAAC-----GAATCTAAC
         *** ******** ******* *****       ***   ***                ****   *   *             * *  ** **    ** * *         ***  ***

BES11    TATACTGTAGAGCCTGTCTGGGGACCTTTCACGGGAGCGGGGTCCAACGCGGCAGCAATACATTCGAGTGTATCTACCGCTGCACTCTGTTGTTCAGTTTTATTGTTTGGAGTGCTGTGA
BES2     TATACTGCAGAACCGGTCCGGGGACATTTCACGGGAGCGGGGTCCAACGCGGCAGCAGTACATTTGAGTGTTTCTACCGCTGCACTTTGTTTTTCAGTTTTATTGTTGGGAGTGCTGTGA
BES1     TATACTGCAGAACCGGTCCGTGGACCTTTCACGGTAGCGGGGTCCAACACAGTAGCAGTACATTTGAGTGTTTCTACCGCTGCACTTTGTTTTTCAGTTTTATTGTTGGGAGTGCTGTGA
BES4     TATACTGCAGAACCGGTCCGGGGACATTTCACGGGAGCGGGGTCCAACGCGGCAGCAGTACATTTGAGTGTTTCTACCGCTGCACTTTGTTTTTCAGCTTTATTGTTGGGAGTGCTGTGA
BES5     TATACTGCAGAACCGGTCCGGGGACATTTCACGGGAGCGGGGTCCAACGCGGCAGCAGTACATTTGAGTGTTTCTACCGCTGCACTTTGTTTTTCAGCTTTATTGTTGGGAGTGCTGTGA
BES7     TATACTGCAGAACCTGTCCGTGGACCTTTCACGGGAGCGGGGGCCAACACAGTAGCAGTACAGTCGAGTGTTTCTACCGCTGCACTTTGTTGTTCAGCTTTATTGTTGGGAGTGCTGTGA
BES13    TATACTGTAGAACCTGTCCGTGGACCTTTCACGGGAGCGGGGTCCAACACAGTAGCAGTACATTTGAGTGTTTCTACCGCTGCACTCTGTTGTTTAGCTTTATTGTTGGGAGTGCTGTGA
BES14    TATACTGCAGAACCTGTCCGTGGACCTTTCACGGGAGCGGGGTCCAACACAGTAGCAGTACATTTGAGTGTTTCTACCGCTGCACTTTGTCGTTCAGCTTTATTGTTGGGAGTGCTGTGA
BES15    TATACTGCAGAACCTGTCCGTGGACCTTTCACGGGAGCGGGGTCCAACACAGTAGCAGTACAGTCGAGTGTTTCTACCGCTGCACTTTGTTGTTCAGTTTTATTGTTGGGAGTGCTGTGA
BES12    TATACTGCAGAACCTGTCCGTGGACCTTTCACTGGAGCGGGGGCCAATGCGGCAGCAATACATTTGAGTGTTTCTACCGCTGCACTTTGTTGTTCAGCTTTATTGTTGGGAGTGCTGTGA
BES3     TATACTGCAGAGCCTGTCCGTGGACCTTTAACGGGAGCGGGGGCCAACGCGGCAGCAATACATTTGAGTGTTTCTACCGCTGCACTTTGTCGTTCAGCTTTATTGTTGGGAGTGCTGTGA
BES10    TATACTGCAGAGCCTGTCCGTGGACCTTTAACGGGAGCGGGGGCCAACGCGGCAGCAATACATTTGAGTGTTTCTACCGCTGCACTTTGTCGTTCAGCTTTATTGTTGGGAGTGCTGTGA
BES17    TATACTGCAGAGCCTGTCCGTGGACCTTTCACGGTAGCGGGGGCCAACGCGGCAGCAATACATTTGAGTGTTTCTACCGCTGCACTTTGTCGTTCAGCTTTATTGTTGGGAGTGCTGTGA
         ******* *** ** *** * **** *** ** * ******* ****  * * **** **** * ****** ************** ***  ** ** ********* ******** ***
```

B

Comparison of ESAG7 from BES1 and BES7

```
         F  K  D  V  I  R  L  F  A  R  F  Q  E  A  K  N  A  V  M  T  K  I  K  T  T  V  D  E  L  T  K  C  I  G  Q  K  E  A  E  L
BES7     TTTAAGGATGTCATTCGCCTGTTTGCGCGCTTCCAAGAAGCAAAAAATGCAGTGATGACGAAAATAAAAACTACTGTGGATGAATTGACGAAATGCATAGGGCAGAAGGAGGCTGAGCTC
BES1     TTTAAGGATGTCATCCGCCTGTTTGCGCGCTTCCAAGAAGCAAAAAATGCAGTGATGAATAAAATAAAAACTACTGTGGATGAATTGGCGAAATGCATAGGGCAGAAAGAGGTTGAGCTC
F1        F  K  D  V  I  R  L  F  A  R  F  Q  E  A  K  N  A  V  M  N  K  I  K  T  T  V  D  E  L  A  K  C  I  G  Q  K  E  V  E  L

         T  N  D  Q  L  Y  E  E  F  I  W  E  T  I  N  R  L  E  L  S  K  R  V  S  E  Q  P  S  L  G  E  E  E  E  T  I  L  K  S  N
BES7     ACTAATGATCAGCTTTACGAGGAATTTATCTGGGAGACCATAAACAGATTGGAGCTGTCAAAGAGAGTGAGTGAACAACCCTCTTTAGGTGAAGAAGAGGAGACGATCCTGAAATCTAAC
BES1     ACTAATGATCAGCTTTACGAAGAATTC------GAGGCAATA----------------CAAAAGTACCTAGGG--------TCTCTGTGAAATGGAGTAAAGGC------GAATTC-AAC
F1        T  N  D  Q  L  Y  E  E  F       E  A  I                 Q  K  Y  L  G         S  L  *                          N

         Y  T  A  E  P  V  R  G  P  F  T  G  A  G  A  N  T  V  A  V  Q  S  S  V  S  T  A  A  L  C  C  S  A  L  L  L  G  V  L  *
BES7     TATACTGCAGAACCTGTCCGTGGACCTTTCACGGGAGCGGGGGCCAACACAGTAGCAGTACAGTCGAGTGTTTCTACCGCTGCACTTTGTTGTTCAGCTTTATTGTTGGGAGTGCTGTGA
BES1     TATACTGCAGAACCGGTCCGTGGACCTTTCACGGTAGCGGGGTCCAACACAGTAGCAGTACATTTGAGTGTTTCTACCGCTGCACTTTGTTTTTCAGTTTTATTGTTGGGAGTGCTGTGA
F1        Y  T  A  E  P  V  R  G  P  F  T  V  A  G  S  N  T  V  A  V  H  L  S  V  S  T  A  A  L  C  F  S  V  L  L  L  G  V  L  *
```

Figure S1

```
BES7-6.      MMRFWFVLLALLGKETY--AYENERNALNATAANKVCGLSTYLKGIAHRVNSESAVVTEK     58
BES7-7       -MRFLFVLLALLGKETHANYYENERNALNATAANKVCALSTYLKGIAHRVNSESAVVTEK     59
              *** ***********:   *****************.**********************

BES7-6       LSDLKMRSIQLQLSVMRNRVPSGEKDCKDIRTLLKTVLRNEFTFQQELEEMRSASALAAA     118
BES7-7       LSDLKMRSIQLQLSIMRNRVPSGEKDCKDIRTLLKTVLRNEFTFQQELEEVRNASALAAA     119
             **************:************************************:*.*******

BES7-6       AAGLAAGRLEEWIFVFAQAADGSSQFCISVGKTIPAEHGDLQECFDGKIGPETLYKIEDS     178
BES7-7       AAGLAAGRLEEWIFVFAQAGGRSSQFCISTGKTGPAEYNNLQECFDGTIGPETLYKIEDS     179
             *******************.. *******.*** ***:.:*******.************

BES7-6.      RVKESAQKSLQLHEVLSSISFGSLGVKNIVEKGENRGCNLMRTADEGLLKDVC-LNRNFT     237
BES7-7       RVKESAKTRLLLHEVLSSISFSSLGAENIRGGNGKDGCNLVRTDNNGILKGGSPTRHNLT     239
             ******:. * **********.***.:**   . : ****:** ::*:**. .  .:*:*

BES7-6       WGGGVLNFGYCVAGNLKIKGGEYGDVSSYDAVRWTEDPSKVSIFKDVIRLFARFQEAKNA     297
BES7-7       WGGGVMNFGSYQNGSMYVEGGEYGDATEYGAVRWTEDPSKVSIFKDVIRLFARFQEAKNA     299
             *****:***    *.: ::******.:.*.******************************

BES7-6       VMTKIKTTVDELTKCIGQKEAELTNDQLYEEFIWETINRLELSKRVSEQPSLGEEEETIL     357
BES7-7       VMTKIKTTVDELTKCIGQKEAELTNDQLYEEFIWETINRLELSKRVSEQPSLGEEEETIL     359
             ************************************************************

BES7-6       KSNYTAEPVRGPFTGAGANTVAVQSSVSTAALCCSALLLGVL     399
BES7-7       KSNYTAEPVRGPFTGAGANTVAVQSSVSTAALCCSALLLGVL     401
             ******************************************


# NetGPI 1.1      Timestamp: 20240925160446
# ID  Seq-length  Pred. GPI-Anchored      Omega-site pos.   Likelihood  Amino-acid
Sequence    399        GPI-Anchored      372                   0.438          G

ESAG6
# SignalP-6.0     Organism: Eukarya Timestamp: 20250215202022
# ID  Prediction  OTHER SP(Sec/SPI) CS Position
Sequence    SP    0.000369    0.999614    CS pos: 17-18. Pr: 0.9774

ESAG7
# SignalP-6.0     Organism: Eukarya Timestamp: 20250215202326
# ID  Prediction  OTHER SP(Sec/SPI) CS Position
Sequence    SP    0.000332    0.999656    CS pos: 18-19. Pr: 0.9760
```

Figure S2

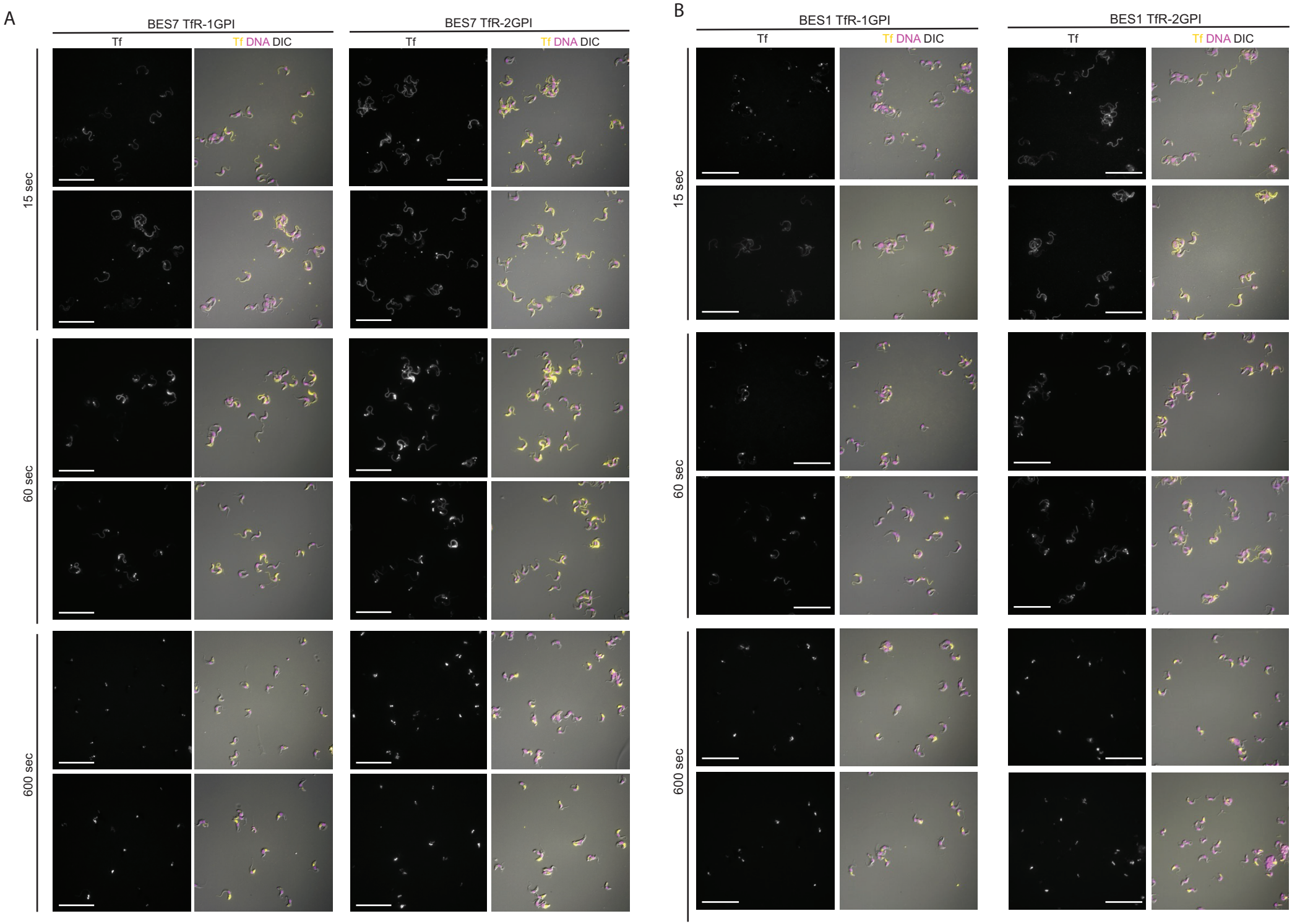
A
BES7 TfR-1GPI
BES7 TfR-2GPI
Tf
Tf DNA DIC
15 sec
60 sec
600 sec
B
BES1 TfR-1GPI
BES1 TfR-2GPI
Tf
Tf DNA DIC
15 sec
60 sec
600 sec

Figure S3

A

```
cow      -DPERTVRWCTISTHEANKCASFRENVLRILESGPFVSCVKKTSHMDCIKAISNNEADAV    59
dog      VSPEKTVRWCTVSNHEASKCSSFMENMKTVLENGPFVSCVKRTSYLECIKAIWANEADAV    60
          .**:******:*.***.**:** **:  :**.********:**:::*****  ******

cow      TLDGGLVYEAGLKPNNLKPVVAEFHGTKDNPQTHYYAVAVVKKDTDFKLNELRGKKSCHT    119
dog      TLDAGLVFEAGLNPYNLKPVVAEFYGKD--KQTRYYAVAVVKKSSTFNLNQLQGKKSCHT    118
         ***.***:****:* *********:*..   **:*********.: *:**:*:*******

cow      GLGRSAGWNIPMGKLYKELPDPQESIQRAAANFFSASCVPCADQSSFPKLCQLCAGKGTD    179
dog      GLGRSAGWNIPMGLLYWKLPEPRESLQKAASSFFTASCVPCVDRTAFPKLCQLCVGKGTD    178
         ************* ** :**:*:**:*:**:.**:******.*:::********.*****

cow      KCACSNHEPYFGYSGAFKCLMEGAGDVAFVKHSTVFDNLPNPEDRKNYELLCGDNTRKSV    239
dog      KCACSNHEPYFGYSGAFKCLMEDAGEVAFVKHSTVLENLPNKADLDQYELLCPDNKRKPV    238
         **********************.**:*********::****  * .:***** **.** *

cow      DNYQECYLAMVPSHAVVARTVGGKEDVIWELLNHAQEHFGKDKPDNFQLFQSPHGKDLLF    299
dog      GEYKQCYLAKVPSHAVVARSVGGKEDLIWELLNQAQEHYGKDKSKVFQLFSSTLGKDLLF    298
         .:*::**** *********:******:******:****:**** . ****.*  ******

cow      KDSADGFLKIPSKMDFELYLGYEYVTALQNLRESKPPDSSKDECM-VKWCAIGHQERTKC    358
dog      KDSAEGFFRIPPKMDTWLYLGYEYVTALRNLREDVRPDTPRDECKKVKWCAVGHHEIAKC    358
         ****:**::** ***  ***********:****.  **: :***  *****:**:* :**

cow      DRWSGFSGGAIECETAENTEECIAKIMKGEADAMSLDGGYLYIAGKCGLVPVLAENYKTE    418
dog      DEWSVNSEGKIECESAESTEDCIAKIAKGEADAMSLDGGYIYIAGQCGLVPVLAENYKTQ    418
         *.**  * * ****:**.**:***** *************:****:*************:

cow      DGSCKNTPEKGYLAVAVVKTSDANINWNNLKGKKSCHTAVDRTAGWNIPMGLLYSKINNC    478
dog      GSTCSNTAEEGYLAVAVVKELDKTISWNNLQGRKSCHTAVDRTAGWNIPMGLLYNRINHC    478
         ..:*.** *:*********  * .*.****:*:**********************.:**:*

cow      KFDEFFSAGCAPGSPRNSSLCALCIGSEKGTGKECVPNSNERYYGYTGAFRCLVEKGDVA    538
dog      EFDKFFSQGCAPGSMRNSSLCALCIGSANVPGKECVPNNHERYYGYTGAFRCLVEKGDVA    538
         :**:*** ****** ************ :  *******.:********************

cow      FVKDQTVIQNTDGNNNEAWAKNLKKENFEVLCKDGTRKPVTDAENCHLARGPNHAVVSRK    598
dog      FVKDQTVLQNTGGKNTEDWAKDLKEEDFELLCPDGQRKSVDKAPECFLAKAPNHAVVSRK    598
         *******:***.*:*.* ***:**:*:**:** ** ** * .* :*.**:.*********

cow      DKATCVEKILNKQQDDFGKSVTDCTSNFCLFQSNSKDLLFRDDTKCLASIAK-KTYDSYL    657
dog      DKASCVSKMLLDQQLLFGRNGNDCSGKFCLFHSATKDLLFRDDTQCLAKLPEDTTYKSYL    658
         ***:**.*:* .**  **:. .**:.:****:* :*********:***.: : .**.***

cow      GDDYVRAMTNLRQCSTSKLLEACTFHKP   685
dog      GAEYITAVANLRQCSTSKLLEACTFHTS   686
         * :*: *::*****************.

Identities
501/686
```

B

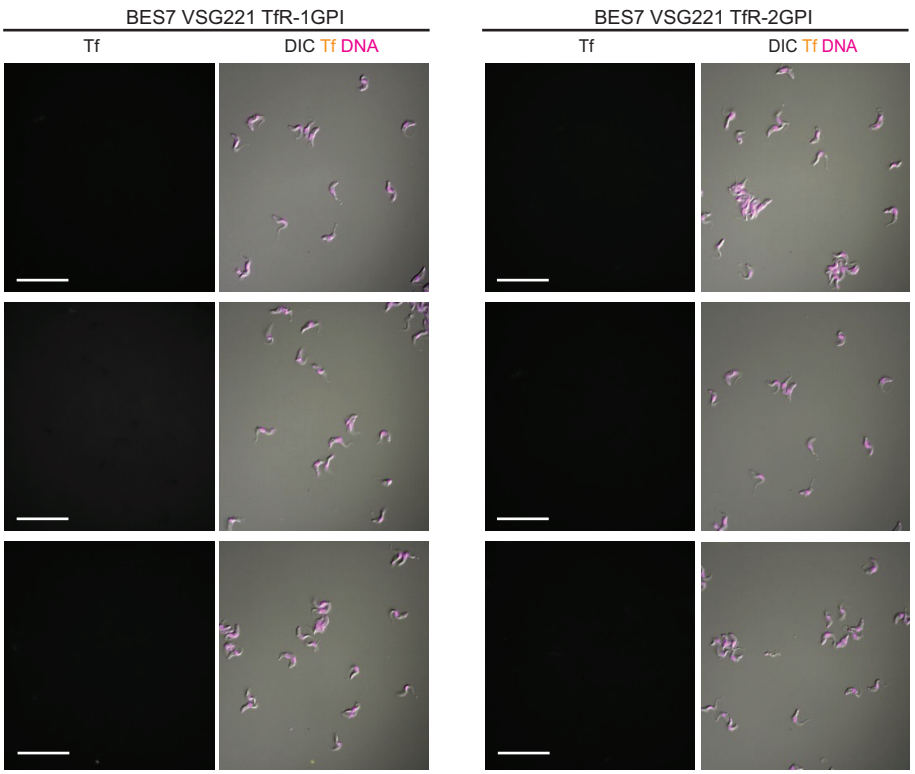

Figure S4

C

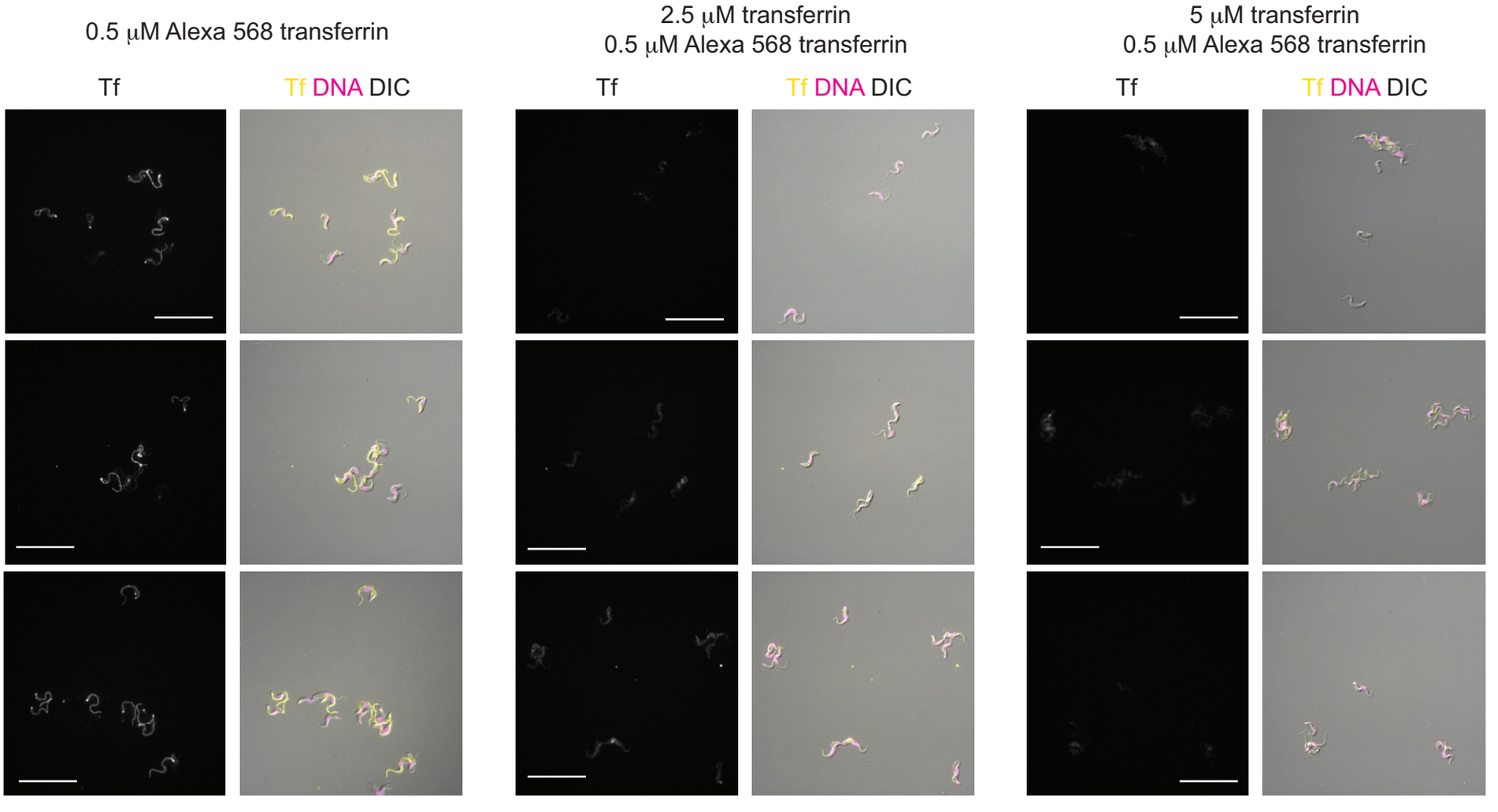
0.5 μM Alexa 568 transferrin
Tf
Tf DNA DIC
2.5 μM transferrin
0.5 μM Alexa 568 transferrin
Tf
Tf DNA DIC
5 μM transferrin
0.5 μM Alexa 568 transferrin
Tf
Tf DNA DIC

Figure S4

D

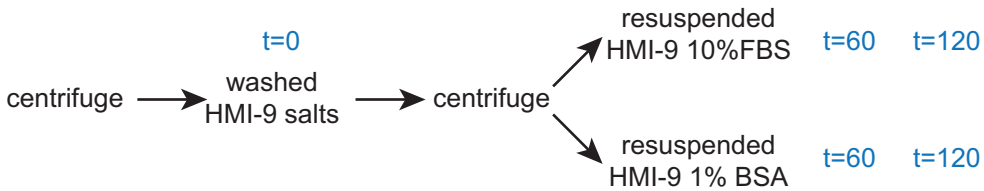
t=0
centrifuge
washed
HMI-9 salts
centrifuge
resuspended
HMI-9 10%FBS
t=60
t=120
resuspended
HMI-9 1% BSA
t=60
t=120

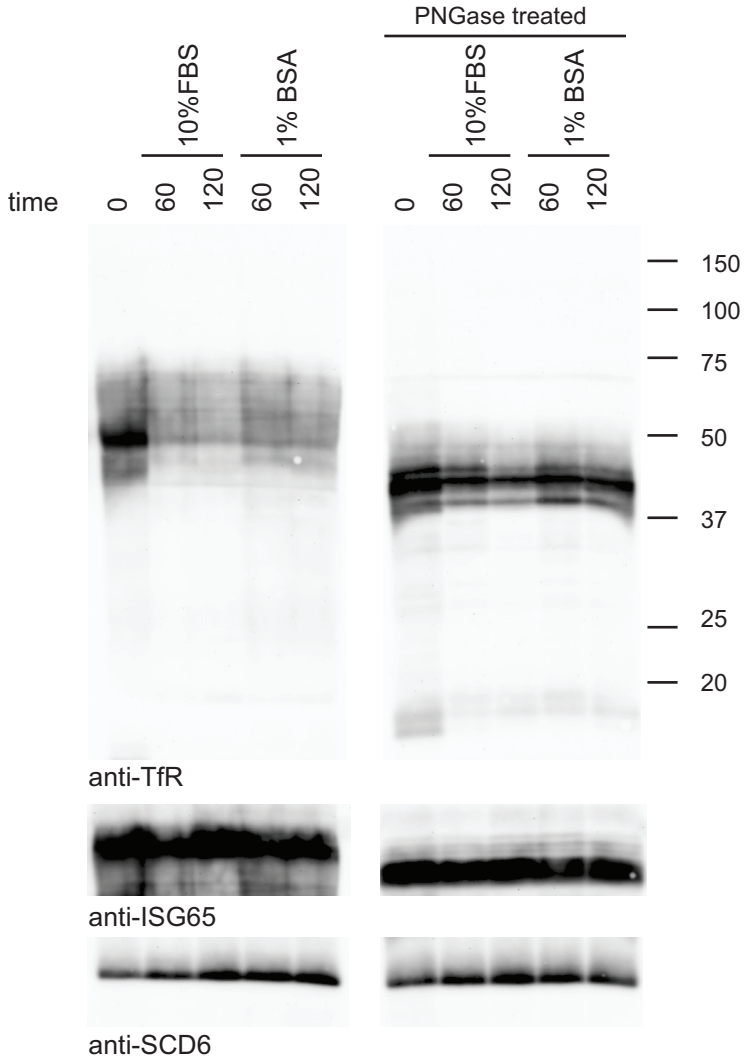
PNGase treated
10%FBS
1% BSA
10%FBS
1% BSA
time
0
60
120
60
120
0
60
120
60
120
150
100
75
50
37
25
20
anti-TfR
anti-ISG65
anti-SCD6

Figure S4

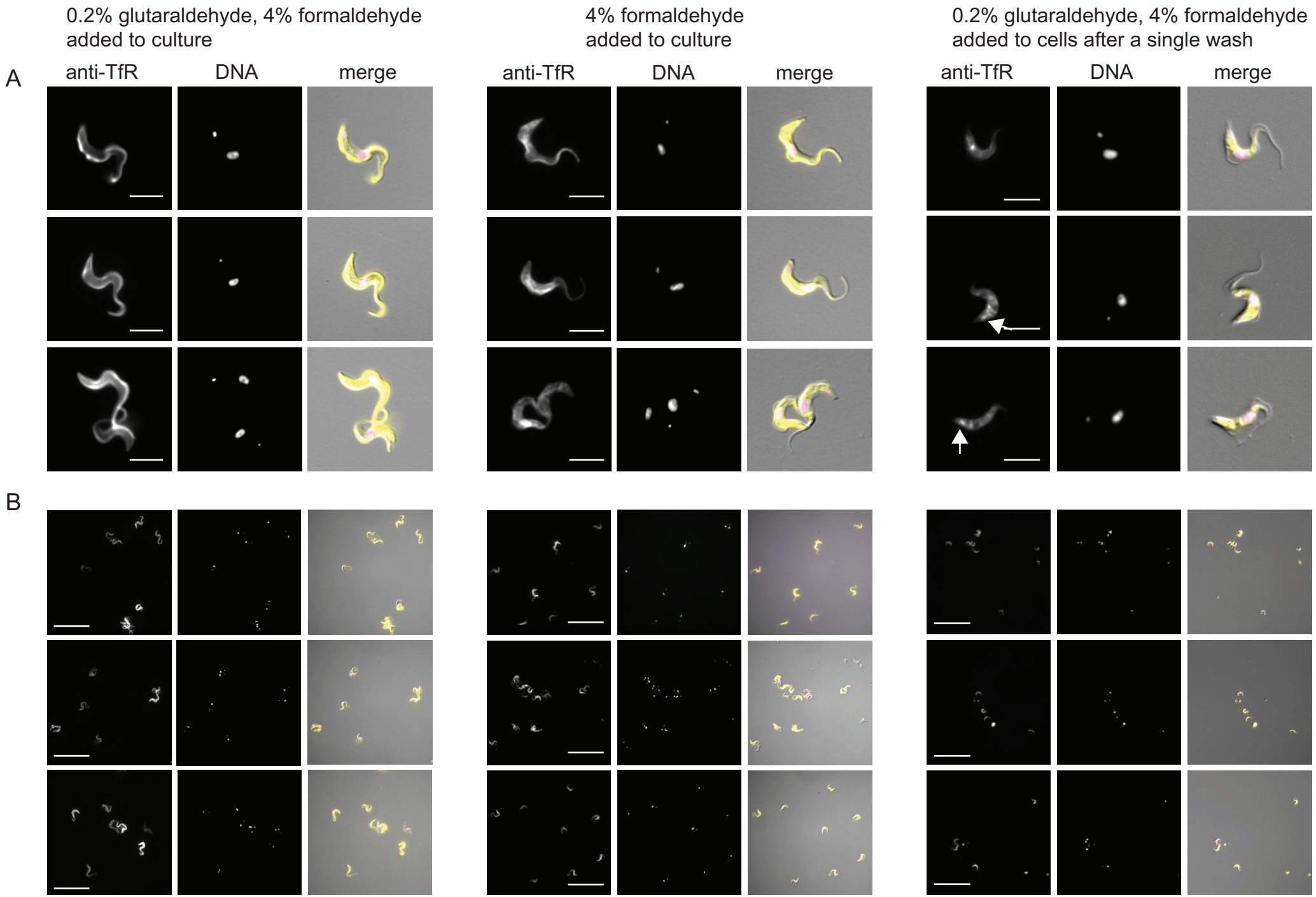
0.2% glutaraldehyde, 4% formaldehyde added to culture
4% formaldehyde added to culture
0.2% glutaraldehyde, 4% formaldehyde added to cells after a single wash
A
anti-TfR
DNA
merge
B

Figure S5

C

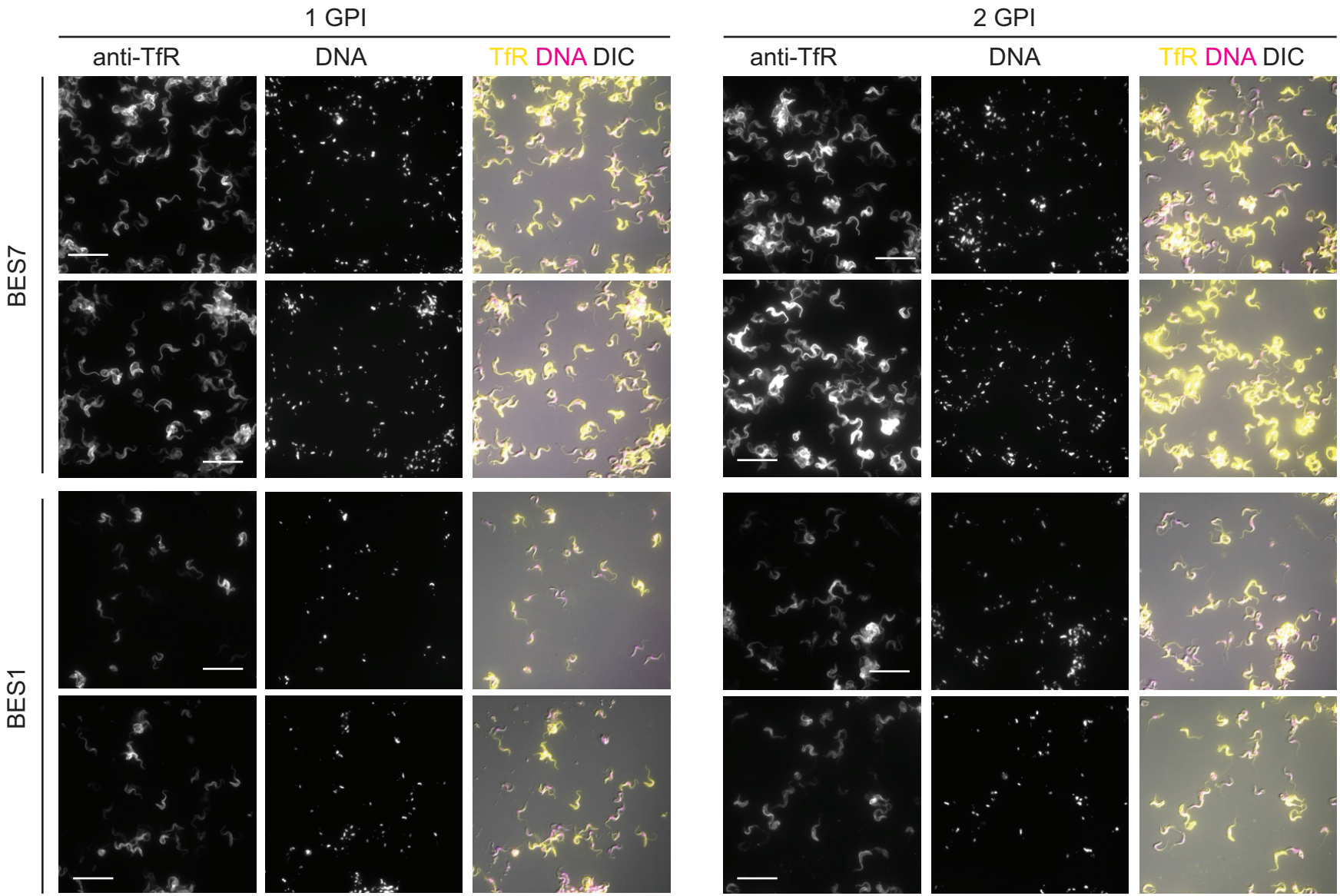
1 GPI
2 GPI
anti-TfR
DNA
TfR DNA DIC
anti-TfR
DNA
TfR DNA DIC
BES7
BES1

Figure S5

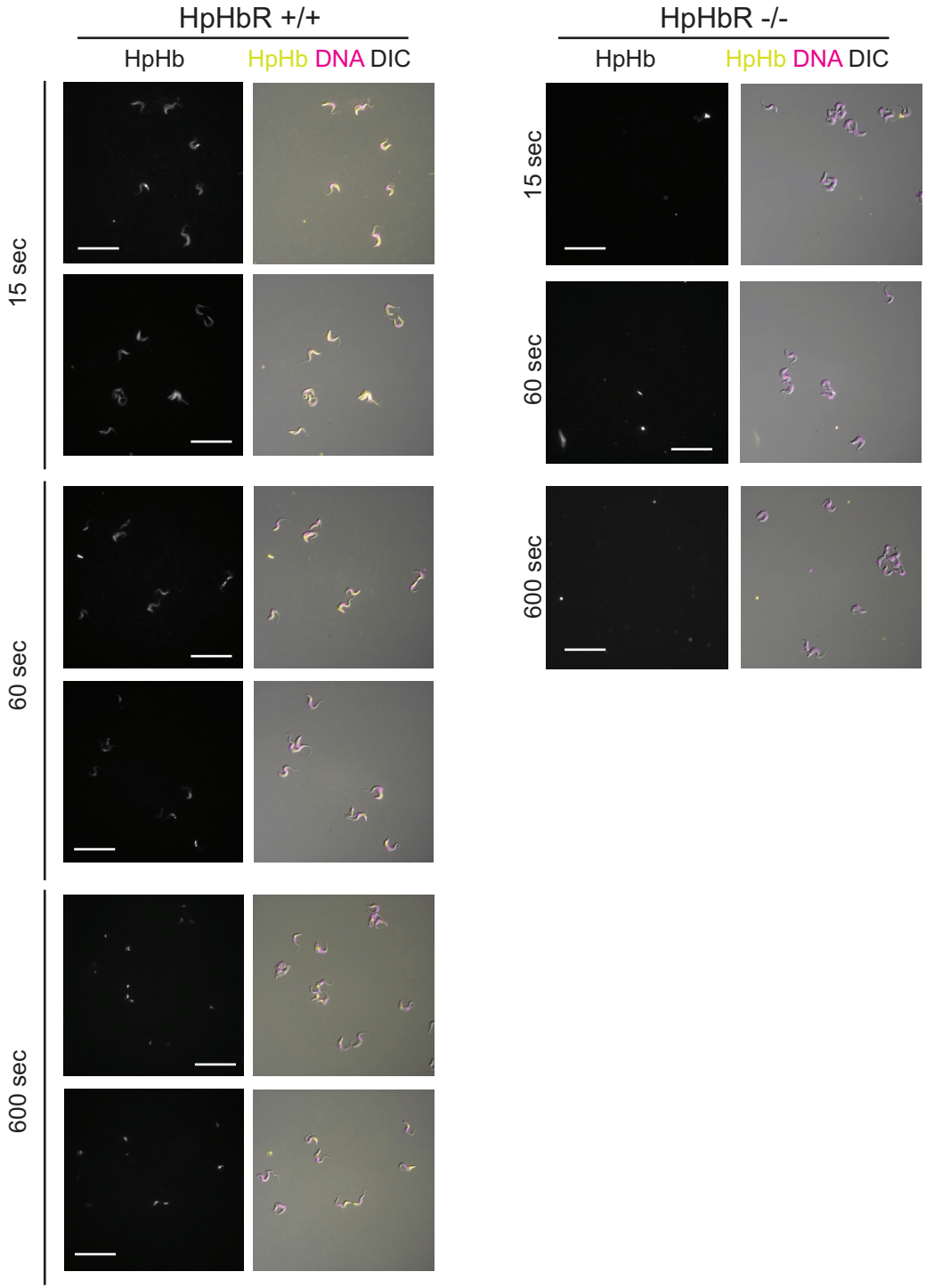
HpHbR +/+
HpHbR -/-
HpHb
HpHb DNA DIC
HpHb
HpHb DNA DIC
15 sec
60 sec
600 sec
15 sec
60 sec
600 sec

Figure S6

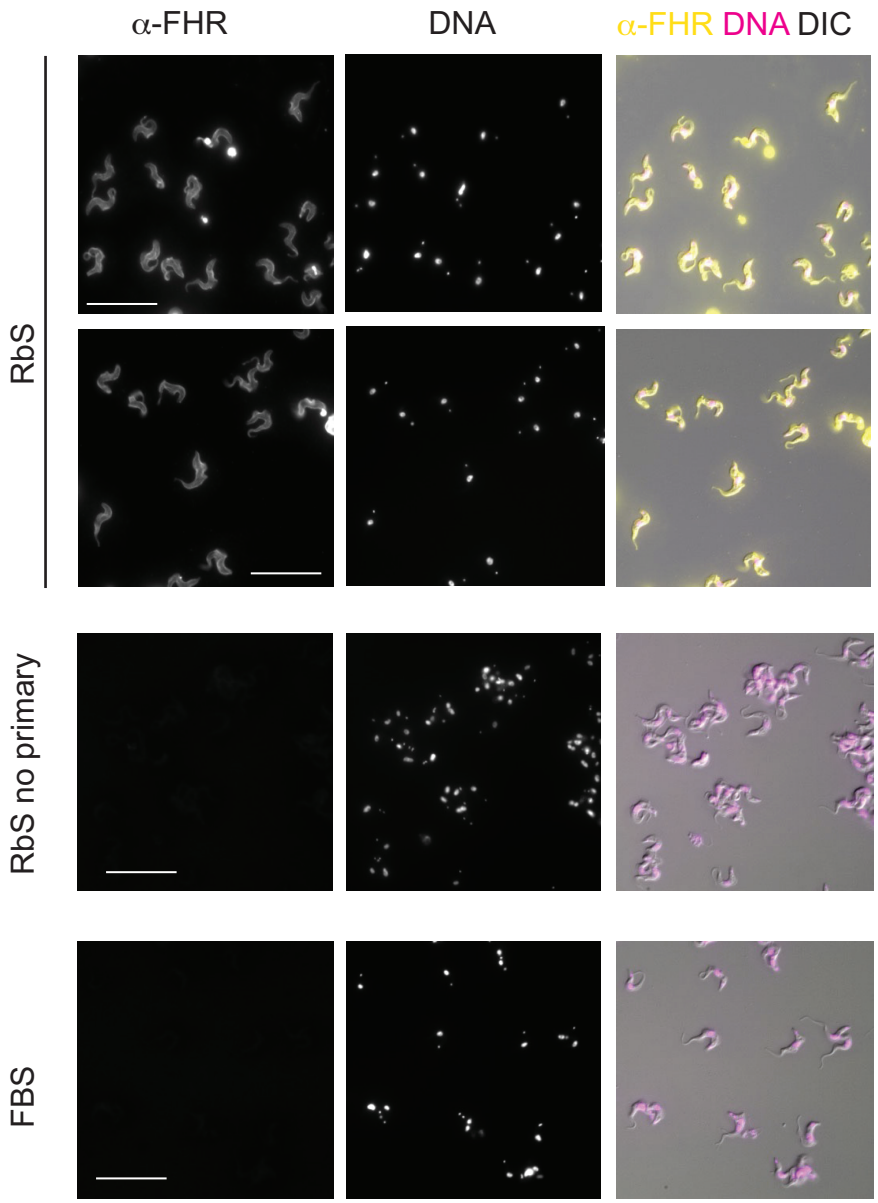

Figure S7